PNAS
www.pnas.org

Supplementary Information for

Programming colloidal bonding using DNA strand-displacement circuitry

Xiang Zhou[a,†], Dongbao Yao[a,†,*], Wenqiang Hua[b], Ningdong Huang[c], Xiaowei Chen[c], Liangbin Li[c,*], Miao He[a], Yunhan Zhang[a], Yijun Guo[a], Shiyan Xiao[a,*], Fenggang Bian[b,*], and Haojun Liang[a,*]

[a]CAS Key Laboratory of Soft Matter Chemistry, Hefei National Laboratory for Physical Sciences at the Microscale, *i*ChEM (Collaborative Innovation Center of Chemistry for Energy Materials), University of Science and Technology of China, Hefei, Anhui 230026, P. R. China; [b]Shanghai Synchrotron Radiation Facility, Zhangjiang Laboratory, Shanghai Advanced Research Institute, Chinese Academy of Sciences, Shanghai 201204, P. R. China; [c]National Synchrotron Radiation Lab, CAS Key Laboratory of Soft Matter Chemistry, University of Science and Technology of China, Hefei, Anhui 230026, P. R. China.

[*]Email: hjliang@ustc.edu.cn, dbyao@ustc.edu.cn, xiaosy@ustc.edu.cn, bianfenggang@zjlab.org.cn, or lbli@ustc.edu.cn.

[†]X.Z. and D.Y. contributed equally to this work.

This PDF file includes:

www.pnas.org/cgi/doi/10.1073/pnas.1917941117

S1. Materials and methods

S1.1. Materials

All DNA molecules used in this work (Tables S1-S6) were designed with the help of NUPACK software (1) to avoid any undesired secondary structures and then synthesized by Sangon Biotechnology Co., Ltd. (Shanghai, China). The 10 nm citrate-capped gold nanoparticles (AuNPs) used in all the experiments were obtained from nanoComposix (San Diego, USA). *Corynebacterium glutamicum* (*Cg*) catalase was purchased from Sigma-Aldrich. Tris (2-carboxyethyl) phosphine hydrochloride (TCEP) was obtained from Alfa Aesar. 4S GelRed dye was also purchased from Sangon Biotechnology Co., Ltd. (Shanghai, China). Other chemicals were of analytical grade and were purchased from Sinopharm Chemical Reagent Co., Ltd. (China) unless otherwise indicated. Ultrapure water (18.2 MΩ·cm) (Millipore Co., USA) was used in all the experiments. All DNA molecules except the thiol-terminated oligonucleotides were dissolved in 0.5 M phosphate-buffered saline (PBS, 0.5 M NaCl, 10 mM sodium phosphate).

S1.2. Preparation of the dual hybridized DNA substrate used in DNA strand-displacement circuit

For construction of the DNA strand-displacement circuit, the preparation of a dual hybridized DNA complex, named *Substrate*, as shown in Fig. S1, with sufficient purity is generally required. All DNA substrates used in this work were manually purified by nondenaturing polyacrylamide gel electrophoresis (PAGE) to remove imperfect hybridized structures according to a previously reported method with a slight modification (2). Briefly, each single strand included in *Substrate*, *Trigger*, *By-product* and *Bottom-substrate* was combined in an appropriate stoichiometry at molar concentrations of ~50 μM and treated with thermal annealing, wherein the solutions were heated to 95 ℃ for 10 min and slowly cooled to room temperature. Before purification, a *Fuel* strand (shown in Fig. S6A) was added to hybridize with poorly formed *Substrate* complexes to form double-stranded products that can be distinguished from correct-structure *Substrate*s via a nondenaturing PAGE gel. Then, the samples premixed with 33% glycerol in a volume ratio of 5:1 were run on a 12% nondenaturing PAGE gel at 240 V for 6 hours using a Hoefer standard vertical electrophoresis unit (Hoefer, Inc., San Francisco, CA, USA). Afterwards, the gel was removed and stained with 4S GelRed dye (Sangon Biotechnology). The desired bands were removed from the gel under UV light, cut into small pieces, and then soaked in 0.5 M PBS for 2 days at 4 ℃. Next, the solution was extracted, and the gel pieces were removed using an Ultrafree-MC centrifugal filter (0.45 μm, Millipore). The purified *Substrate* was quantitated by measuring the absorbance at 260 nm on a UV-vis spectrophotometer (Agilent, Cary 300, USA).

S1.3. Preparation of DNA linkers used in building "programmable atom equivalents" (PAEs)

To construct PAEs with active sticky ends (*PAE*) and deactivated PAEs with protected sticky ends (*dPAE*) involved in our system, DNA linkers with different architectures, such as *Duplex-linker* and *Dual-duplex-linker* with active sticky ends and *Duplex-linker'* and *Dual-duplex-linker'* with protected sticky ends (Fig. S2), need to be prepared first. Notably, *Dual-duplex-linker* is an extended *Duplex-linker* with an additional double-stranded region. These DNA linkers were prepared by combining the single DNA strands involved with an equal molar ratio, 1:1 for *Duplex-linker* and *Duplex-linker'* and 1:1:1 for *Dual-duplex-linker* and *Dual-duplex-linker'*, followed by thermal annealing, in which the linkers were heated to 95 ℃ for 10 min and then slowly cooled to

room temperature. These formed DNA linkers were directly used for building PAEs without further purification.

S1.4. Preparation of DNA-functionalized AuNPs (DNA-AuNPs)

To construct the PAEs (*PAE* and *dPAE*), DNA-AuNPs were first prepared according to the procedures in previous literature reports (3, 4) (Fig. S3). Briefly, thiol-terminated oligonucleotides were reduced with 100 mM TCEP for one hour, and excess TCEP was removed via a NAP-5 column (GE Healthcare). Activated thiolated DNA strands were then added to AuNP colloids in a molar ratio of approximately 300:1 and incubated at 4 ℃ overnight. Afterwards, 2% sodium dodecyl sulfate (SDS) and 200 mM sodium phosphate (pH = 7.4) were added to the solution in sequence to bring the final concentrations of SDS and sodium phosphate to 0.01% and 10 mM, respectively. Then, a "salt aging" process was conducted by the stepwise addition of 4 M NaCl over 2 days. After a final salt concentration of 0.5 M NaCl was reached, the solution was allowed to equilibrate overnight to achieve maximum DNA loading. Unbound DNA strands were then removed by three rounds of centrifugation (13500 rpm, 60 min) and 0.5 M PBS with 0.01% SDS was used as the cleaning buffer. After the last round of centrifugation and removal of the supernatant, the precipitate was resuspended in 0.5 M PBS. The concentration of DNA-AuNPs can be estimated by measuring the absorbance at 520 nm on a UV-vis spectrophotometer.

S1.5. Estimation of DNA loading on AuNPs

To quantify the number of thiolated DNA strands on each AuNP, DNA strands were first modified with 1-hexanethiol and the 6-FAM fluorophore at their 5' and 3' ends, respectively. These DNA strands were attached to AuNPs in the same manner as described above. The DNA-AuNP concentration was obtained from a UV-vis spectrophotometer. After that, 2.5 mM DTT was added to a solution of 1 nM DNA-AuNPs in 0.5 M PBS to displace the DNA strands from the AuNP surface. After incubation overnight, the DNA strands were fully released into the solution, inducing the aggregation of the AuNPs. The AuNP precipitate was then removed via a short period of centrifugation, and the fluorescence of the supernatant was measured by a fluorescence spectrophotometer (F-7000, Hitachi). The concentration of the released DNA strands was estimated according to a standard curve of fluorescence intensity as a function of the concentration of fluorescent DNA strands. The number of DNA strands per particle was calculated by dividing the number of released strands by the number of AuNPs. As a result, approximately 80 strands were found to be grafted onto the surface of each AuNP with a diameter of ~10 nm.

S1.6. Preparation of DNA-functionalized proteins (DNA-proteins)

DNA-proteins were prepared according to literature procedures (5, 6) (Fig. S4). A type of the tetrameric heme-containing enzyme, *Cg* catalase with a similar size as 10 nm AuNP, was first exchanged into 100 mM sodium bicarbonate buffer (0.5 M NaCl, pH = 9.0) by ultrafiltration (Pierce Protein Concentrator, 30K MWCO). The absorbance of *Cg* catalase at 405 nm was measured using a NanoDrop 2000 spectrophotometer (Thermo Scientific), and the concentration was then calculated according to its molar extinction coefficient of 324,000 $M^{-1} \cdot cm^{-1}$ (7). Then, 3 mg of the linker NHS-PEG_4-N_3 (Thermo Scientific) in DMSO was added to 100 μL of 20 μM *Cg* catalase. The reaction was conducted at 25 ℃ while shaking at 1,000 rpm on a thermoshaker for

2 hours. The azide-modified proteins were then purified via five rounds of ultrafiltration (Pierce Protein Concentrator, 30K MWCO) and resuspended in 0.5 M PBS. Next, 5'-DBCO-terminated DNA strands in 0.5 M PBS were added to the azide-modified proteins at a molar ratio of approximately 300:1. After incubating at 25 ℃ for 3 days while shaking at 1,000 rpm on a thermoshaker, unbound DNA strands were removed by five rounds of ultrafiltration (Pierce Protein Concentrator, 100K MWCO).

S1.7. Constructions of PAEs

The PAEs with active sticky ends (*PAE*, Fig. S5A) were prepared via the binding between the anchor domain of *Duplex-linker* and the thiolated DNA strand on *DNA-AuNP* and can directly participate in PAE assembly. The duplex region in the middle part of *Duplex-linker* acts as a spacer to adjust the length of *Duplex-linker*. In addition, a nonbonding single base (adenosine, A) was added at both ends of the spacer domain of the *Duplex-linker* to increase the flexibility of the DNA linker and further enhance the crystallization process. The deactivated PAEs (*dPAE*, Fig. S5B) are inaccessible for PAE assembly due to their protected sticky ends. A toehold domain is preserved in *Duplex-linker'* to activate the protected sticky ends through a strand-displacement reaction between the *Trigger* strand and *Duplex-linker'*. Notably, the sticky ends in *dPAE* are only partially covered to balance the efficiency of the strand-displacement reaction and the stability of *dPAE*. For the preparation of *PAE* and *dPAE*, the linkers *Duplex-linker* or *Duplex-linker'* were combined with *DNA-AuNP* at an appropriate molar ratio. The mixture was then heated to 45 ℃ for 5 min and subsequently cooled back to room temperature to ensure that the linkers were fully hybridized onto *DNA-AuNP*. Notably, PAEs with active self-complementary sticky ends do not need to be prepared in advance since the bonding of the sticky ends between PAEs will lead to PAE aggregation immediately once *Duplex-linker* and *DNA-AuNP* are combined.

S1.8. Assembly of PAEs driven by a DNA strand-displacement circuit

Typically, the samples (120 μL) were prepared by combining *dPAE* (25 nM) with the DNA *Substrate* and *Fuel* strand in 200-μL PCR tubes, to which *Substrate* and *Fuel* in the DNA circuit were added in two-fold and four-fold amounts of *Duplex-linker'*, respectively. Then, varied amounts of the *Catassembler* strand were introduced into the sample solution to initiate the operation of the DNA strand-displacement circuit, thus leading to the release of the *Trigger* strand that subsequently induced the PAE assembly.

S1.9. PAE assembly via thermal annealing

PAE aggregates were formed via cooperative interactions of sticky ends between PAEs in a 200-μL PCR tube. For all systems, the aggregation of PAEs was complete in approximately one hour at 25 ℃. After that, the PAE aggregates in 0.5 M PBS were heated to temperatures around their melting temperatures (T_m), followed by slow cooling to 25 ℃ at a rate of 0.1 ℃/min using a PCR thermal cycler (Applied Biosystems, Veriti, USA). To determine the melting temperature, the PAE aggregates in 0.5 M PBS were transferred to a cuvette with the addition of a tiny magneton. Subsequently, the cuvette was placed into the thermal control module of the UV-vis spectrophotometer, and then the sample was heated from 25 ℃ to 65 ℃ at a rate of 0.25 ℃/min while continuously stirring. The melting curve of the PAE aggregates was recorded by monitoring

the temperature-dependent absorbance of the AuNPs at 520 nm. The T_m of the PAE aggregates was defined as the temperature corresponding to the maximum value in the first derivate of the melting curve. Typically, the measured values of T_m were ~44 ℃ for the unary system (Fig. 1E), ~36 ℃ for the binary system (Fig. S16F), and ~31 ℃ for the asymmetric binary system (Fig. 2F) mentioned in the main text.

S1.10. Small angle X-ray scattering (SAXS) experiments

The PAE aggregates prepared via DNA circuit-driven assembly or annealing were transferred to 1.0-mm quartz capillary tubes (Sinopharm Chemical Reagent Co., Ltd) for SAXS measurements. All SAXS experiments were performed at the BL16B1 beamline of the Shanghai Synchrotron Radiation facility (SSRF) with X-rays at a wavelength of 1.24 Å (10 keV). The sample-to-detector distance was determined using cowhells as a standard. The 2D scattering patterns were collected by a detector, and the typical exposure time for the aggregates was set as 5 seconds. 1D scattering data were obtained by taking a radial average of the 2D scattering patterns using Fit2D software, generating profiles of scattering intensity as a function of scattering vector q: $q = 4\pi \sin\theta / \lambda$, where θ is half of the scattering angle 2θ and λ is the X-ray wavelength. In a SAXS measurement, the scattering signals from the capillary tube and the scattering of the DNA and buffer were negligible relative to that of PAE aggregates. The measured scattering intensity I(q) can be regarded as the product of the form factor P(q) and the structure factor S(q), where P(q) is the scattering related to the size and shape of the PAEs and S(q) represents the scattering related to the arrangement of PAEs in aggregates. The form factor was obtained by collecting the SAXS data from completely dispersed PAEs. The theoretical X-ray diffraction patterns in this work were calculated with the *PowderCell* software that is available free of charge from the Federal Institute for Materials Research and Testing (www.ccp14.ac.uk/ccp/web-mirrors/powdcell/a_v/v_1/powder/e_cell.html).

S2. Supplementary Text

S2.1. The detailed reaction processes of the DNA strand-displacement circuit and the corresponding fluorescence kinetic characterization

In the main text, we provided a simplified description of the reactions occurring in the DNA strand-displacement circuit; the detailed steps are shown here in Fig. S6A. Specifically, the system that comprises two components, the dual hybridized DNA *Substrate* and *Fuel* strand, is initially stable. Upon addition of the *Catassembler* strand b*-a*, domain a* can bind with its complementary toehold (domain a) in *Substrate* to produce an *Intermediate-1* complex. *By-product* strand c*-b* in *Substrate* is displaced in the first round of the toehold-mediated strand-displacement reaction (TMSDR) to produce *Intermediate-2*, and then the *By-product* strand leaves automatically, leading to exposure of domain c in the produced *Intermediate-3*. Domain c serves as a toehold in the new round of TMSDR between *Fuel* and *Intermediate-3*, which results in a *Waste* complex and release of two strands: *Catassembler* that is reusable to reinitiate the reaction of the DNA circuit and *Trigger* e*-d* that initiates assembly of "programmable atom equivalents" (PAEs).

The performance of the DNA strand-displacement circuit was investigated via fluorescence kinetic measurements. The DNA circuit consisting of *Substrate*, *Fuel* and *Catassembler* was operated as described above (Fig. S6A). The *Trigger* strand was released gradually from the circuit. In addition, the fluorescent *Reporter* was prepared by hybridization of quencher (BHQ2)-labeled strand d* with fluorophore (Cy5)-labeled strand d-e, resulting in quenching of Cy5 fluorescence. The released *Trigger* strand was hybridized with strand d-e, followed by the displacement of strand d* in *Reporter* through the TMSDR and the emergence of fluorescence signal. The real-time fluorescence kinetics of the operation of the DNA circuit were measured by a fluorescence spectrophotometer (F-7000, Hitachi). As shown in Fig. S6B, the *Trigger* release kinetics displayed obvious delayed behavior with a decrease in the amount of *Catassembler* added (from 10 to 0 nM).

S2.2. The principle of PAE assembly programmed by the DNA strand-displacement circuit and the corresponding aggregation kinetics characterization

A scheme of PAE assembly driven by the DNA strand-displacement circuit using a time-dependent interaction strategy is shown in Fig. S8A. The scheme consists of two cascaded subsystems, in which the first subsystem (also see Fig. S6A) is responsible for releasing *Trigger* strand e*-d* to initiate PAE assembly of the second subsystem. Here, we show the example of the unary system. The deactivated PAE (*dPAE*) used in the unary system was prepared as shown in Fig. S7, in which the strand f-d-e-m (*Linker*) is protected by a partially complementary strand d*-f_1* (*Protector*). Since the sticky end (domain f) is covered, *dPAE* is deactivated at this stage.

Upon adding the *Catassembler* strand b*-a*, it follows the reaction process described in Fig. S6A to generate the *Trigger* strand e*-d* that subsequently displaces the *Protector* strand to expose the self-complementary sequence of domain f in *dPAE* to yield active self-complementary sticky ends, thereby resulting in self-assembly and formation of ordered PAE lattices.

The kinetics of PAE assembly in a unary system driven by the DNA strand-displacement circuit was studied using the kinetics module of a UV-vis spectrophotometer (Fig. S8B). The assembly rate of PAEs gradually decreased with decreasing *Catassembler* concentration, which demonstrated that the kinetics of PAE assembly can be finely regulated by the catassembly DNA circuit.

S2.3. The effect of linker density on PAE crystallization

According to previous studies (3, 8), linker density plays an important role in PAE crystallization, including crystal quality and crystallographic symmetry. In this study, we investigated the effect of linker density on crystallization by altering the ratio of *Duplex-linker'*/*DNA-AuNP* in the unary system (Fig. S9). Pronounced FCC small angle X-ray scattering (SAXS) peaks appeared at *Duplex-linker'*/*DNA-AuNP* ratios of from 22:1 to 40:1, which means an appropriate density of linker shell is required to form a well-assembled ordered structure. Consider that in addition to the attractive force arising from DNA base pairing, there exist various types of repulsive interactions between DNA shells, including charge repulsion from negatively charged DNA chains, excluded volume repulsion, and repulsion from the conformational entropy of DNA chains (9-12), all of which are highly relevant to the density of DNA shells on PAEs. The attractive force dominates, and the repulsive force contributes less when the density is low. As the density grows, the repulsive force that avoids mutual contact between PAEs plays such a key role that the attractive force is unable to balance the repulsive force, resulting in the formation of more disordered aggregates. Therefore, the ratio of *Duplex-linker'*/*DNA-AuNP* was set at 30:1 in the unary system described in the main text (Fig. 1). In addition, PAE crystallization behaviors in the unary system when the molar ratios of *Duplex-linker'*/*DNA-AuNP* were 40:1, 50:1, and 60:1 were also investigated via both the thermal annealing strategy and the time-dependent interaction scheme (Fig. S10). In these systems, the FCC lattices gradually formed as the concentration of *Catassembler* decreased from 50 to 0.5 nM, and these lattices exhibited similar crystal structures to those formed after thermal annealing.

S2.4. Effect of linker length on PAE crystallization

As the size of PAEs is determined by both the size of the inner nanoparticle core and the length of the outer-layer DNA linkers, the time-dependent interaction strategy was applied to construct PAE lattices having varied lattice parameters by changing the length of the DNA linker. Typically, in a unary system, a variable length of poly-dA sequence h* was hybridized to a complementary poly-dT domain h in the linker to adjust the linker length (Fig. S11A). Then, PAE assembly was performed with the same principle as described in Fig. S8A. As indicated by the 1D and 2D SAXS data shown in Fig. S11B, FCC lattices formed, and in the 1D SAXS patterns of these lattices, the shift in the positions of the first-order scattering peak (q_0) to smaller values of q with increasing DNA linker length mean the increase in the size of the lattice cell, according to the equation:

$$D = \sqrt{6}\pi \, / \, q_0$$

where D is the distance between two nearest-neighbor nanoparticle used to dictate the size of the lattice cell and q_0 is the position of the first-order scattering peak.

S2.5. Kinetics of PAE lattice formation

Kinetics experiments for PAE lattice formation in the unary system using the time-dependent interaction scheme were performed. Typically, a series of parallel samples were prepared and kept at 25 ℃ for different times before SAXS measurements.

As shown by the curves from 0 to 8 hours in Fig. S12, the temporal evolution of the SAXS model indicated that the weak attraction among PAEs in the early assembly stage could not

produce detectable PAE aggregates when less *Trigger* strand was released from the catassembly DNA circuit. The emergence of the typical FCC SAXS peaks at 12 hours means the generation of ordered lattices arising from the increased attractive force between PAEs as more *Trigger* strands were released (Fig. S12).

S2.6. The strategy of manual addition of *Trigger*

In order to confirm the mechanism of the time-dependent interaction scheme, we designed a control experiment to manually add the *Trigger* strands slowly drop by drop over time to simulate the release process of *Trigger* from the DNA circuit. To this end, we first obtained three standard fluorescence kinetic curves (slow, medium, and fast release) by adding 2, 5, and 50 nM *Catassembler* to the DNA circuit characterized by a fluorescent *Reporter* to track the actual amounts of the *Trigger* strands released into the solution at different times over a period of 24 hours (Fig. S13A). According to the fluorescence intensities of these curves, we calculated the actual release amounts of *Trigger* at different time points marked on these curves. As shown in Fig. S13A, when 50 and 5 nM *Catassembler* were added, almost all of the *Trigger* strands (1.4 μM of the entire 1.5 μM *Trigger* that hybridized to *Substrate*) were released from the *Substrate* in 1 and 24 hours, respectively; when a 2 nM *Catassembler* was added, incomplete release (0.9 μM) occurred within 24 hours. Because 0.75 μM *Trigger* strands (the same number with the protected sticky ends on the *dPAE*) are sufficient to induce complete assembly of PAEs, thus PAEs were assembled into FCC lattice in the presence of 2 nM *Catassembler* (Figs. S8B and S13B).

For the strategy of manual addition, the *Trigger* strands were stepwise added into the PAE assembly system over time according to the actual release amounts of the *Trigger* strands at different time points marked in the kinetic curves (Fig. S13A). As shown in Fig. 13C, the fast addition of *Trigger* (a total amounts of 1.4 μM *Trigger* strands were added at the beginning) led to a rapid assembly of PAEs and the formation of disordered PAE aggregates ("Fast" curve in Fig. S13C); the addition of *Trigger* at a medium rate, 1.4 μM *Trigger* strands were dropwise added in 12 times over 24 hours, resulted in the formation of FCC structure (lines of "Medium" in Fig. S13C); and the slow addition of *Trigger* (0.9 μM *Trigger* strands were dropwise added in 12 times over 24 hours) induced the formation a more ordered FCC lattice.

Additionally, another control experiment was also performed to slowly introduce the *Duplex-linker* manually into a solution containing only DNA-AuNPs. Similar with the manual addition of *Trigger*, the fast addition of the total amounts of 750 nM *Duplex-linker* at once at the beginning (the molar ratio for *Duplex-linker* and *DNA-AuNP* was 30:1) induced disordered PAE aggregates (Fig. S13D). However, the manual addition of the same amounts of *Duplex-linker* at slow (750 nM *Duplex-linker* was added in 4 times in 4 hours) and medium (750 nM *Duplex-linker* was added in 12 times in 12 hours) rates still didn't induce the formation of ordered FCC lattice (Fig. S13D).

Note that similar FCC structures of PAE assemblies were obtained using the strategy of manual addition of *Trigger* compared with the approach of DNA circuit-controlled release of *Trigger* (Fig. S13B and C), which confirmed the mechanism of the time-dependent interaction scheme in constructing of PAE lattices.

S2.7. PAE assembly in the binary system

For PAE assembly in the binary system driven by the DNA strand-displacement circuit with the time-dependent interaction strategy, the design of the catassembly DNA circuit remained

unchanged from that in the unary system. Typically, to prepare two components of deactivated PAEs (*dPAE-1* and *dPAE-2*), two DNA duplex complexes (*Duplex-linker-1'* and *Duplex-linker-2'*) with equal sequence lengths were hybridized to two sets of DNA-functionalized gold nanoparticles (DNA-AuNPs) (*DNA-AuNP-1* and *DNA-AuNP-2*) in the same ratio (Fig. S14). The sticky ends ($^{3'}$−TTCCTT$^{5'}$ and $^{3'}$−AAGGAA$^{5'}$) in each linker were partially protected by the complementary protector strands (*Protector-1* strand d*-g_1* and *Protector-2* strand d*-g_1).

Schemes of PAE crystallization in the binary system via the thermal annealing strategy and time-dependent interaction scheme are shown in Fig. S15. For the assembly of two components of PAEs in the time-dependent interaction strategy, the *Trigger* strands released from the catassembly DNA circuit can simultaneously react with *dPAE-1* and *dPAE-2* and displace *Protector-1* and *Protector-2*. The two non-self-complementary sticky ends are then exposed, thereby resulting in the assembly of the PAEs. The SAXS data in Fig. S16 exhibit BCC lattices formed through both the thermal annealing strategy and time-dependent interaction scheme under different linker density conditions.

Alternatively, we have another method for realizing time-dependent interaction-based PAE assembly in the binary system (Fig. S17). The strategy described above was slightly modified by selectively protecting one of the sticky ends of the two sets of PAEs to obtain *dPAE-1* and *PAE-2* (Fig. S17A). The slightly modified binary system of PAE assembly was also initially stable, and the assembly of the PAEs proceeded upon the addition of *Catassembler*. The SAXS pattern in Fig. S17B indicated that BCC lattices can also be well formed using the modified strategy.

S2.8. Conditional initiation of PAE assembly via selective activation of PAE bonding

An earlier report (3) has demonstrated that the number of DNA linkers on PAEs and the size ratio between two PAEs dictate the thermodynamically favored crystal structure in the binary system. Since the size of PAEs refers to the overall hydrodynamic radius that consists of the nanoparticle core radius and DNA shell thickness, we constructed an asymmetric binary system by functionalizing DNA-AuNPs with non-self-complementary sticky-end DNA linkers of different lengths. Specifically, *PAE-2* of small size was grafted with *Duplex-linker*, and *PAE-1* of large size was grafted with *Dual-duplex-linker*, in which *Dual-duplex-linker* is an extended *Duplex-linker* with an additional double-stranded spacer of 26-base poly-dT (domain h) and its complementary sequence poly-dA (strand h*; *Duplexer*), thereby resulting in a larger size of *PAE-1* than *PAE-2* (Fig. S18). The numbers of DNA linkers on *PAE-1* and *PAE-2* were 80 and 40, respectively. With the slight modification of *PAE-1* (*PAE-2*) by covering the sticky end of the g (g*) domain and exposing the e domain, we also prepared *dPAE-1* and *dPAE-2*, respectively (Fig. S18).

The DNA strand-displacement circuit was operated as described above for releasing the *Trigger* strands to drive the PAE assembly. The PAEs of large size involved in the system were set at a molar ratio of 1:4 to the PAEs of small size (*dPAE*-1/*PAE-2* or *PAE-1*/*dPAE-2*). There are two possible ways for initiating PAE assembly: First (left panel of Fig. S19), upon mixing *dPAE-1* and *PAE-2*, the system is stable since the sticky end on *dPAE-1* is covered; upon releasing *Trigger* strands from the DNA circuit, the *Protector-1* strand on *dPAE-1* is displaced, and correspondingly, the DNA molecular structure (*Dual-duplex-linker'*) on *dPAE-1* was converted to the *Dual-duplex-linker* on *PAE-1*, thereby exposing the sticky end and resulting in PAE assembly. Second (right panel of Fig. S19), upon mixing *PAE-1* and *dPAE-2*, the system is stable because the sticky end on *dPAE-2* is covered; after the *Trigger* strand drives reactions in a similar way to the one just described above, the PAEs assemble.

We observed the formation of a BCC lattice, as shown in the left panel of Fig. 2C, using the first method (the left panel of Fig. S19) and the formation of an AlB_2 lattice, as shown in the right panel of Fig. 2C, using the second method (the right panel of Fig. S19). Notably, for the second strategy, individual scattering spots in the 2D SAXS patterns in Fig. S20D can be observed when less *Catassembler* (1 nM) was added, which represented the formation of large crystalline domains of AlB_2 structures.

S2.9. Dynamically converting a binary system into a unary system and structural transformation of PAE lattice from BCC to FCC

In this section, we describe how to dynamically convert a binary system into a unary system, thereby transforming PAE lattices from BCC to FCC. To this end, *PAE-1* grafted with *Duplex-linker-1* and *PAE-2* grafted with *Duplex-linker-2* were prepared first (Fig. S21A), and a BCC lattice was achieved in this binary system via thermal annealing (Fig. S21B), in which the two types of PAEs were first mixed at room temperature for PAE aggregation (generally disordered aggregates). Then, the melting temperature of the obtained PAE aggregates was measured by a UV-vis spectrophotometer. Finally, the PAE aggregates were heated to a temperature around the melting temperature and slowly cooled down to 25 ℃ at a rate of 0.1 ℃/min to obtain the BCC lattice.

Here, we intentionally designed a higher melting temperature of the unary system (T_{m2} ~57 ℃) (Fig. S24) with a self-complementary sticky end of $^{5'}$−TGCGCA$^{3'}$ (the f domain in Figs. S22 and S23) and a lower melting temperature of the binary system (T_{m1} ~34 ℃) (Fig. S24) with a pair of non-self-complementary sticky ends of $^{5'}$−AAGGAA$^{3'}$ (the g domain in Figs. S22 and S23) and $^{5'}$−TTCCTT$^{3'}$ (the g* domain in Figs. S22 and S23).

We started from the BCC lattice of the binary system produced above to realize the structural transformation into an FCC lattice in two ways: solid-fluid-solid manner and solid-solid manner. First, at a temperature between the two melting points ($T_{m1} < T < T_{m2}$), the BCC lattice was first melted into the fluid state; then, the *Trigger* strand released from the DNA circuit displaced strand d*-g on *PAE-1* and strand d*-g* on *PAE-2* to convert all PAEs to those having self-complementary sticky ends; and finally, the PAEs were assembled into an FCC lattice (Fig. S22). From the corresponding experimental results in Fig. S25, ordered FCC structures can be developed from the initially melted BCC structures (fluid) at a reaction temperature of 40 ℃ as the *Catassembler* concentration decreased (from 50 to 0.5 nM) under programming by the catassembly DNA strand-displacement circuit. Second, at a temperature lower than the melting point of the binary system ($T < T_{m1}$), the *Trigger* strand carrying a self-complementary sticky end released from the catassembly DNA circuit entered the BCC lattice and displaced strand d*-g on *PAE-1* and strand d*-g* on *PAE-2*, by which all PAEs were converted into PAEs having linkers with self-complementary sticky ends and the BCC lattice correspondingly transformed into an FCC lattice in a solid-solid transition manner (Fig. S23). As shown in Fig. S26, the initial BCC structures can be transformed into new FCC structures at reaction temperatures of 25 and 30 °C in the presence of higher concentrations of *Catassembler* (10 and 50 nM). In addition, to further demonstrate the solid-solid transition, we observed the solid-solid transition from BCC to FCC from the *in situ* SAXS measurement results (Fig. S27) by directly adding of 1.5 μM *Trigger* strands (to simulate the fast release of *Trigger* from the cataassembly DNA circuit) into the binary system at 25 °C.

S2.10. Dynamically converting a unary system into a binary system and structural transformation of PAE lattice from FCC to BCC

In this section, we describe how to dynamically convert a unary system into a binary system, thereby transforming PAE lattices from FCC to BCC. In this system, *Duplex-linker-1* hybridized with *DNA-AuNP-1* and *Duplex-linker-2* hybridized with *DNA-AuNP-2* were prepared first. Since these two types of duplex linkers have equal lengths of DNA sequences and the same type of sticky ends, the unary PAE aggregates were obtained by mixing these four components together. Then, the melting temperature of the obtained PAE aggregates was measured by a UV-vis spectrophotometer. Finally, the FCC lattice in this unary system was achieved via a thermal annealing process as mentioned above (Fig. S28).

Here, we intentionally designed a unary system with a lower melting temperature (T_{m1} ~37 ℃) (Fig. S30) with a self-complementary sticky end of $^{5'}$−TAGCTA$^{3'}$ (the f domain in Fig. S29) and a binary system with a higher melting temperature (T_{m2} ~51 ℃) (Fig. S30) and a pair of non-self-complementary sticky ends of $^{5'}$−GGAAGG$^{3'}$ (the g domain in Fig. S29) and $^{5'}$−CCTTCC$^{3'}$ (the g* domain in Fig. S29).

We started from the FCC lattice produced above to realize the structural transformation into a BCC lattice. At a temperature between the two melting temperatures ($T_{m1} < T < T_{m2}$), the FCC lattice was first melted into the fluid state. Then, *Trigger-1* and *Trigger-2* were released from two catassembly DNA circuits bound with *Duplex-linker-1* and *Duplex-linker-2*, respectively, and displaced d*-f strands through TMSDRs to deactivate the existing self-complementary sticky ends on all PAEs (*PAE*), thus resulting in the generation of a pair of new non-self-complementary sticky ends. In this way, the unary PAE system was converted into a binary PAE system, and finally, the new generated PAEs (*PAE-1* and *PAE-2*) were assembled into a BCC lattice (Fig. S29). As shown by the corresponding experimental results in Fig. S31, ordered BCC structures were assembled from dispersed PAEs at 40 ℃ (melted from the initially prepared FCC structures) over a relatively large span of *Catassembler* concentrations (from 400 to 0.5 nM) under programming by two catassembly DNA strand-displacement circuits.

S2.11. Binary AuNP-protein assembly programmed by the DNA strand-displacement circuit

Binary AuNP-protein crystallization was realized according to the procedures described in Fig. S32B. Specifically, *dPAE-1* and *PAE-2* were prepared by mixing *Duplex-linker-1'* and *Duplex-linker-2* with *DNA-AuNP* and *DNA-protein* in an appropriate stoichiometric ratio, respectively (Fig. S32A). These two types of PAEs bearing equal numbers of duplex linkers were then combined in a molar ratio of 1:1. Upon the addition of *Catassembler*, *Trigger* was released from the catassembly circuit and can activate the protected sticky ends on *dPAE-1*, subsequently inducing the assembly of *DNA-AuNP* and *DNA-protein*.

According to a previous study (3), the CsCl crystal structure is thermodynamically favored for the binary AuNP-protein assembly system in principle. However, relative to that of the AuNPs, the scattering of the proteins in the practical SAXS measurements in this work was negligible, thereby resulting in the production of simple cubic scattering patterns, as shown in Fig. S33.

S3. Supplementary Figures

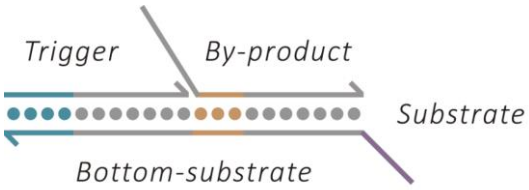

Fig. S1. General scheme of the DNA molecular structure of *Substrate*.

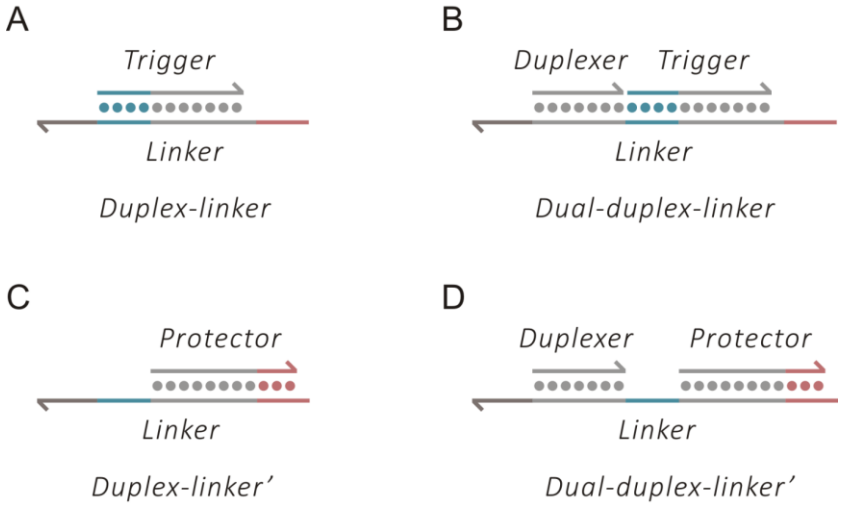

Fig. S2. General schemes of the DNA molecular structures of (A) *Duplex-linker*, (B) *Dual-duplex-linker*, (C) *Duplex-linker'*, and (D) *Dual-duplex-linker'*.

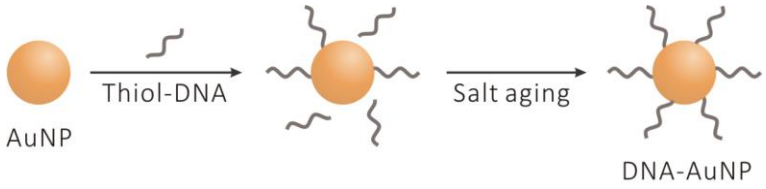

Fig. S3. A schematic of the procedure for preparation of DNA-AuNPs.

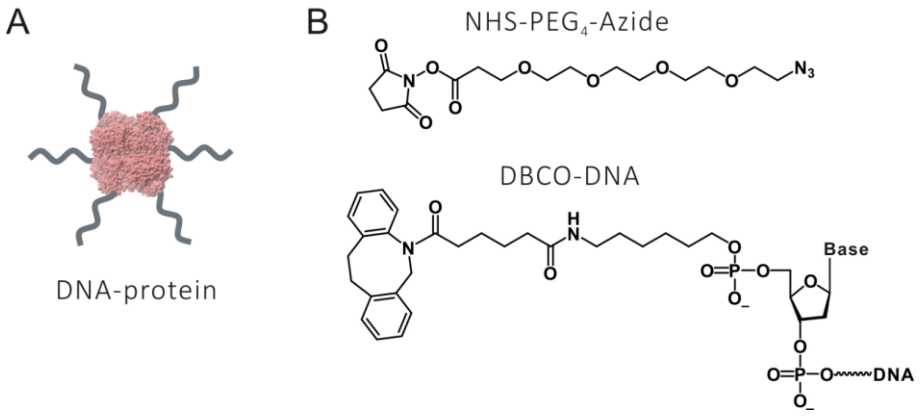

Fig. S4. (A) Schematic of the structure of DNA-protein. (B) The molecular structures of two linker moieties between protein and DNA strand.

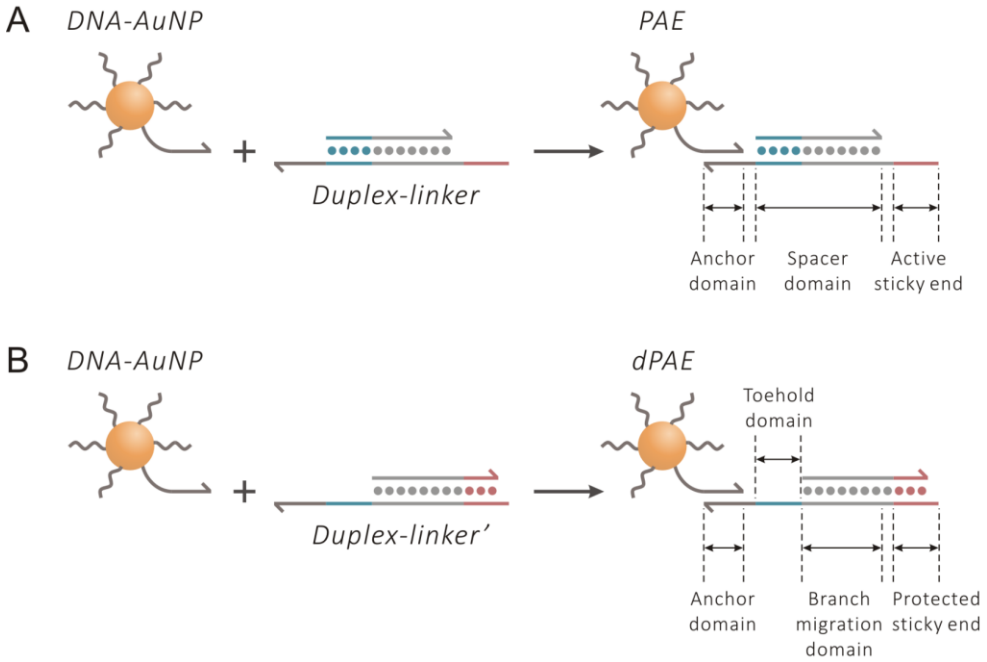

Fig. S5. General schemes for the constructions of PAEs (*PAE* and *dPAE*).

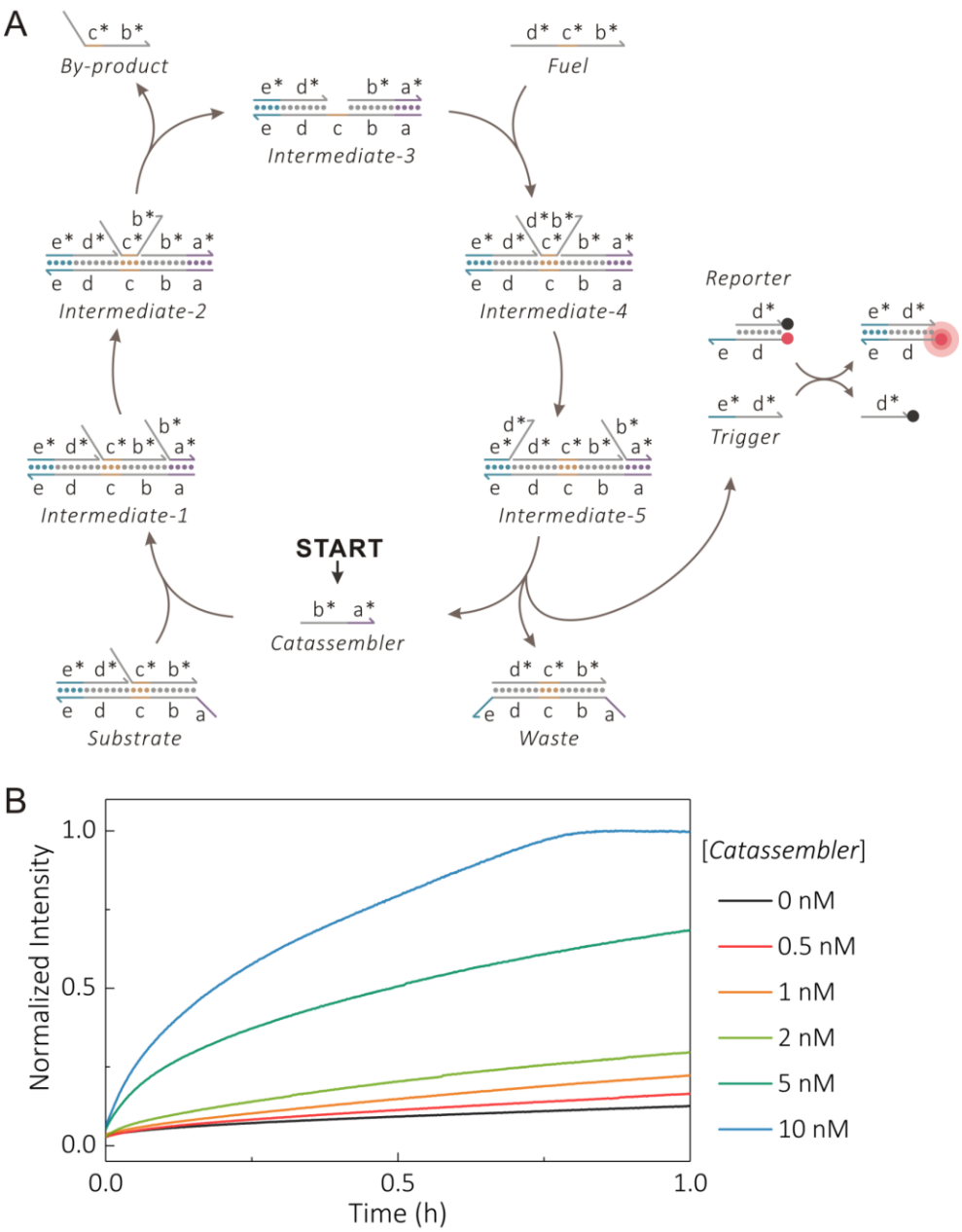

Fig. S6. (A) A schematic of the detailed reaction processes in the DNA strand-displacement circuit. (B) The time-dependent fluorescence kinetics when the concentration of *Catassembler* was varied from 0 to 10 nM. The fluorescence assays were performed with excitation at 645 nm and emission at 663 nm. Here, [*Substrate*] = 1.5 μM, [*Fuel*] = 3 μM, and [*Reporter*] = 0.75 μM.

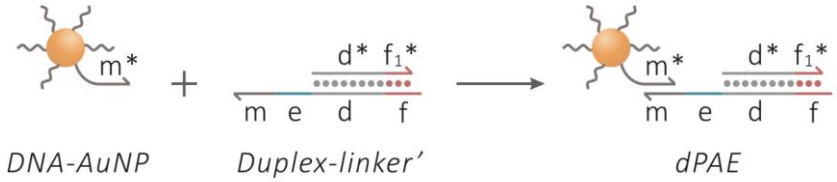

Fig. S7. The construction process of *dPAE* in the unary system programmed by the DNA strand-displacement circuit.

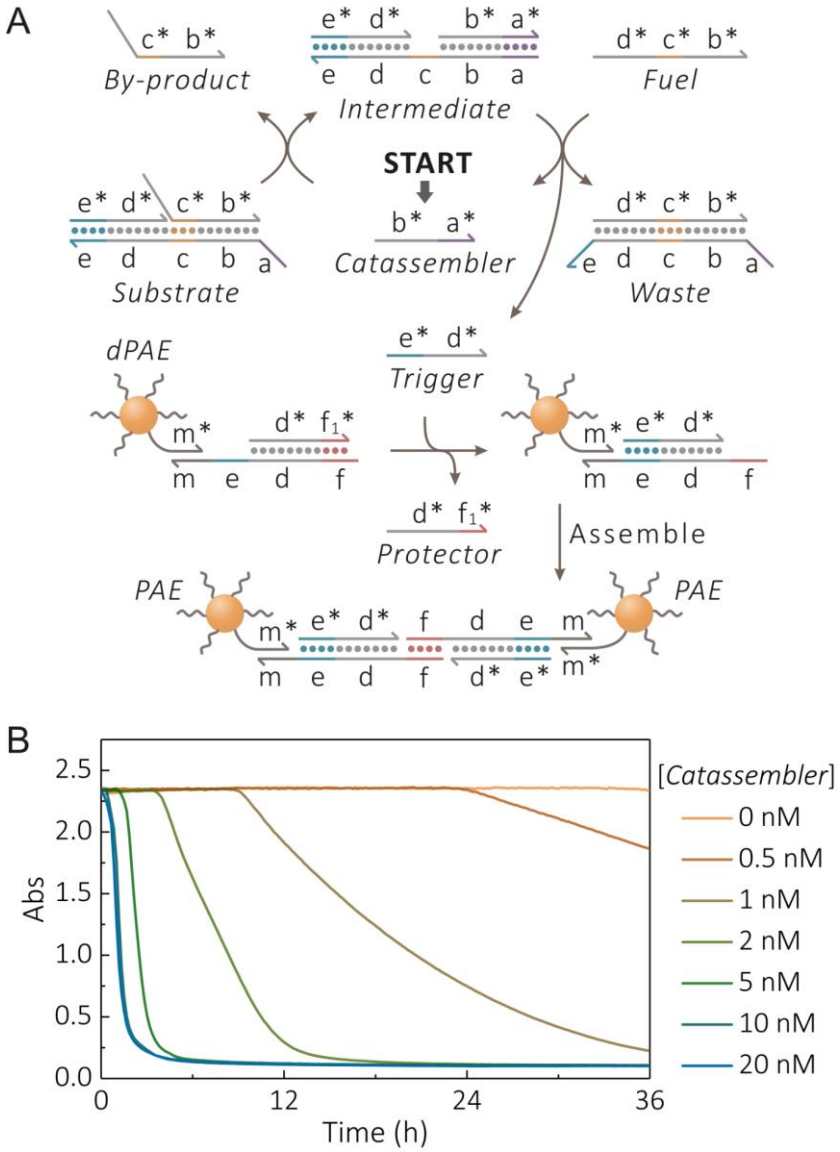

Fig. S8. (A) Schematic representation of PAE assembly driven by the DNA strand-displacement circuit. (B) Kinetics of PAE assembly in the presence of different amounts of *Catassembler*. The ratio of *Duplex-linker'* to *DNA-AuNP* used here was 30:1. [*dPAE*] = 25 nM, [*Substrate*] = 1.5 μM, and [*Fuel*] = 3 μM.

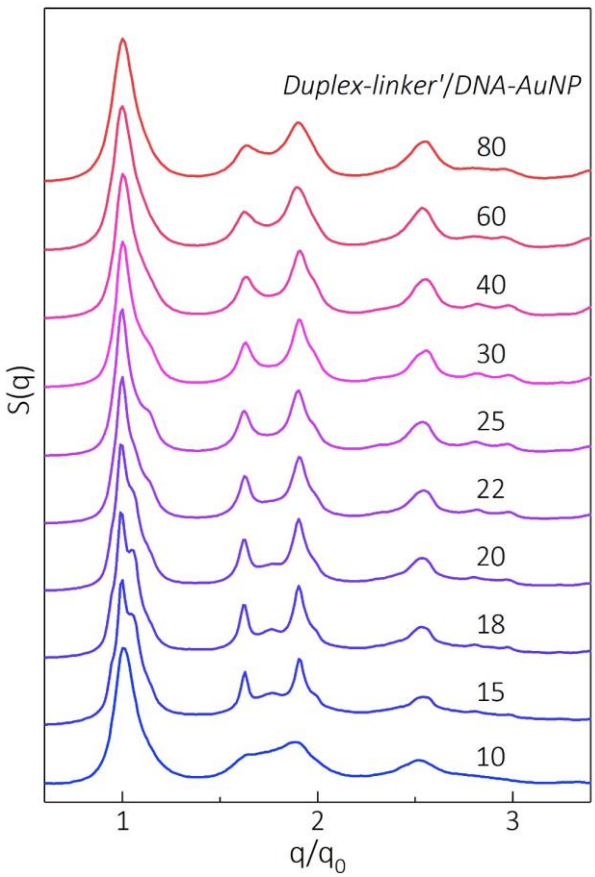

Fig. S9. 1D SAXS patterns of the formed PAE aggregates programmed by the DNA circuit in the unary system as the ratio of *Duplex-linker'*/*DNA-AuNP* was varied from 10 to 80. Here, [*dPAE*] = 25 nM, and each component of the DNA circuit was added at a constant concentration, where [*Substrate*] = 2.8 μM, [*Fuel*] = 5 μM, and [*Catassembler*] = 0.05 nM.

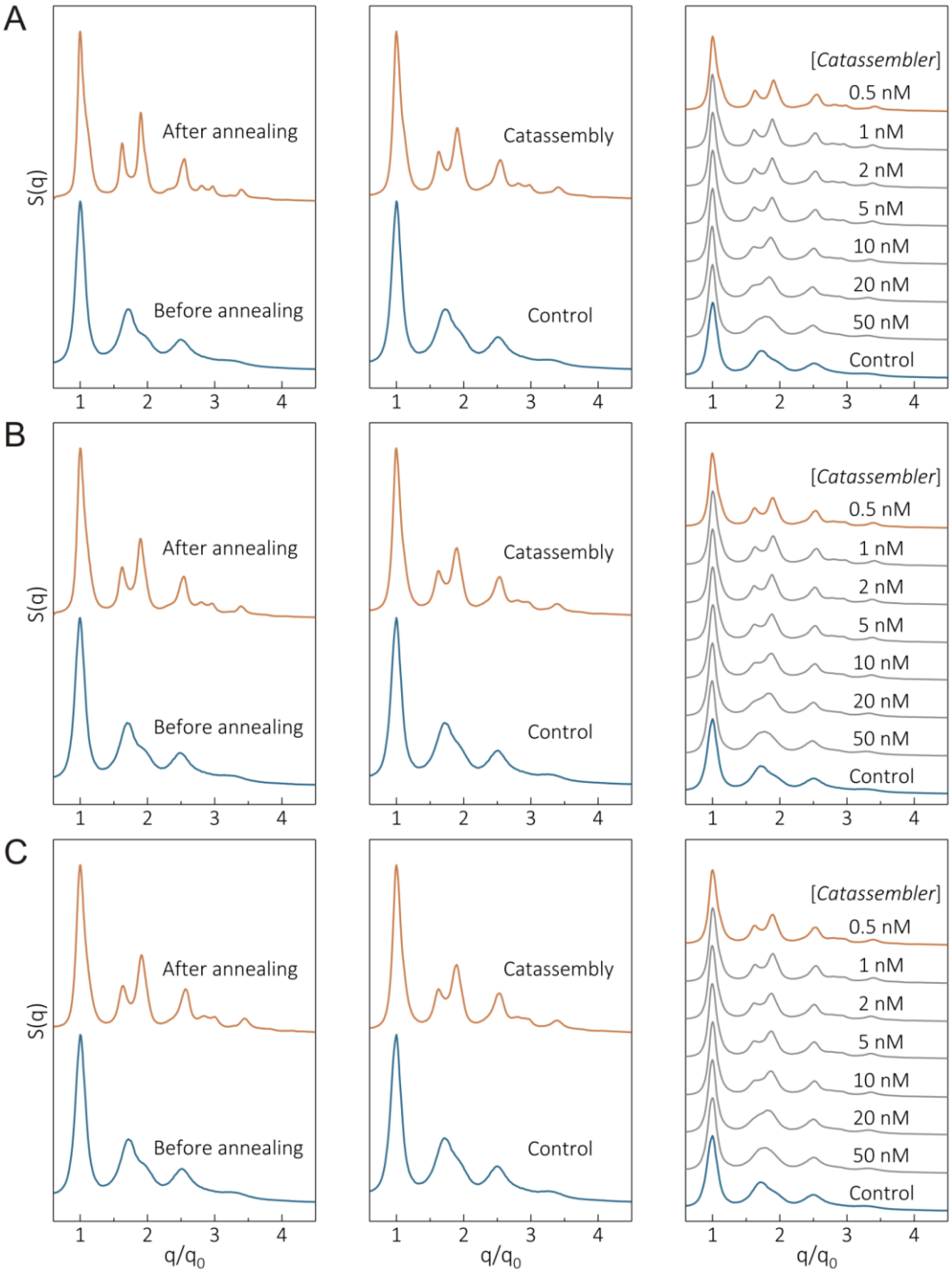

Fig. S10. SAXS measurements of PAE aggregates in the unary system with the ratios of linker/DNA-AuNP at (A) 40:1, (B) 50:1, and (C) 60:1. From left to right, the panels represent 1D SAXS patterns for PAE aggregates formed using a thermal annealing strategy; 1D SAXS patterns for PAE aggregates formed using a time-dependent interaction strategy; and 1D SAXS patterns for PAE aggregates formed with the addition of different amounts of *Catassembler*, respectively. Here, [*PAE*] = 25 nM in the thermal annealing strategy; for the time-dependent interaction scheme, [*dPAE*] = 25 nM, [*Substrate*] = 2× [*Duplex-linker'*], and [*Fuel*] = 2× [*Substrate*].

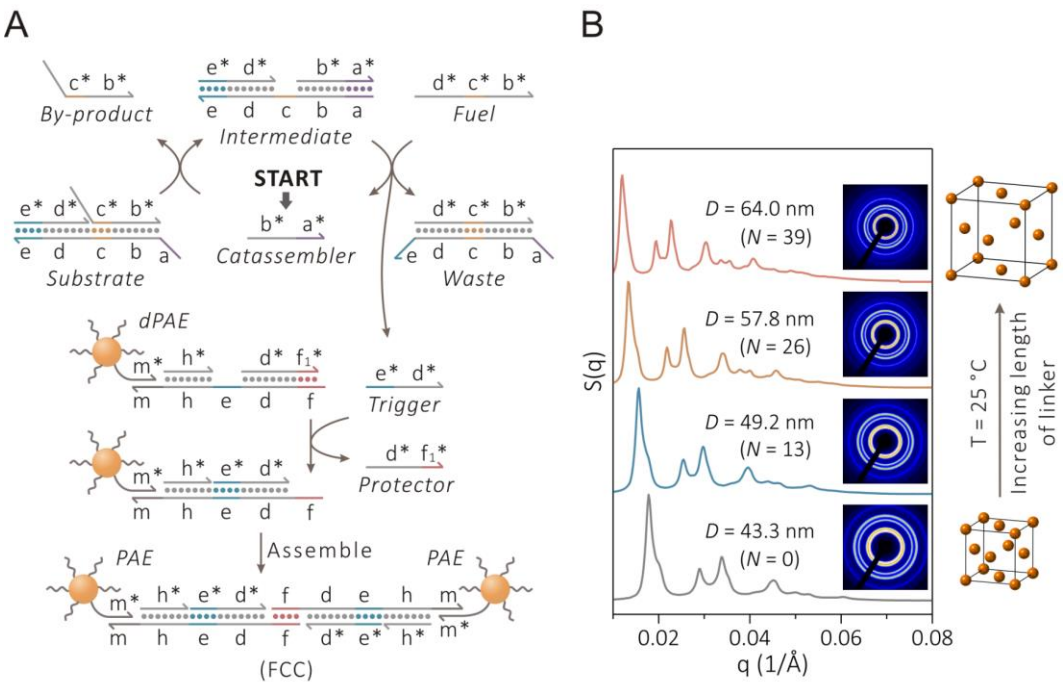

Fig. S11. (A) Scheme of PAE assembly with variable lengths of DNA linkers driven by the DNA circuit in a unary system. (B) 1D and 2D SAXS patterns of FCC lattices constructed by different lengths of DNA linkers and unit cell models of an FCC lattice with different lattice parameters. The numbers (*N*) of base pairs in the h*/h duplex region varied from 0 to 39, the distance (*D*) between two nearest-neighbor nanoparticle was calculated according to the equation above. Here, [*Catassembler*] = 0.5 nM.

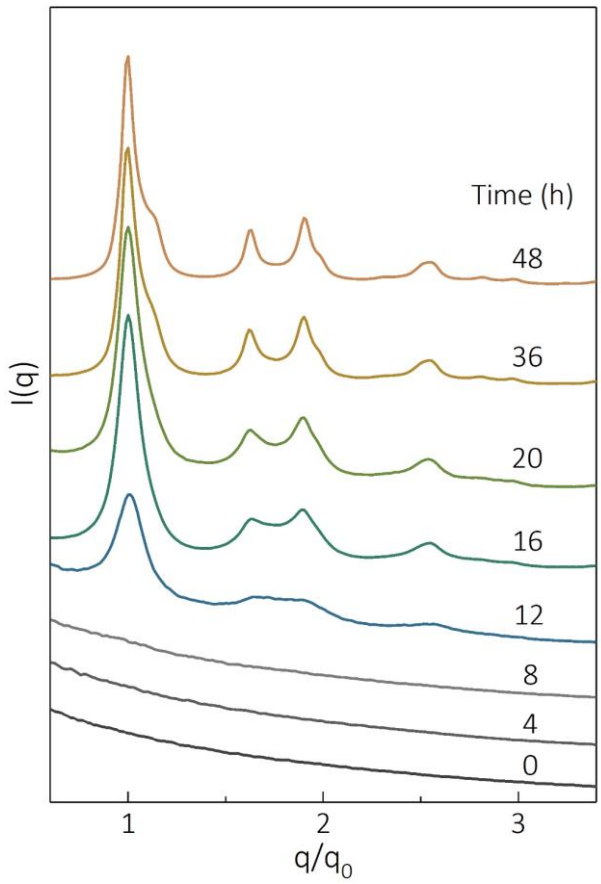

Fig. S12. SAXS patterns measured at different periods of PAE crystallization in a unary system programmed by the DNA circuit. Here, *dPAE* was prepared by hybridizing *Duplex-linker'* and *DNA-AuNP* at a ratio of 30:1, [*Catassembler*] = 0.5 nM.

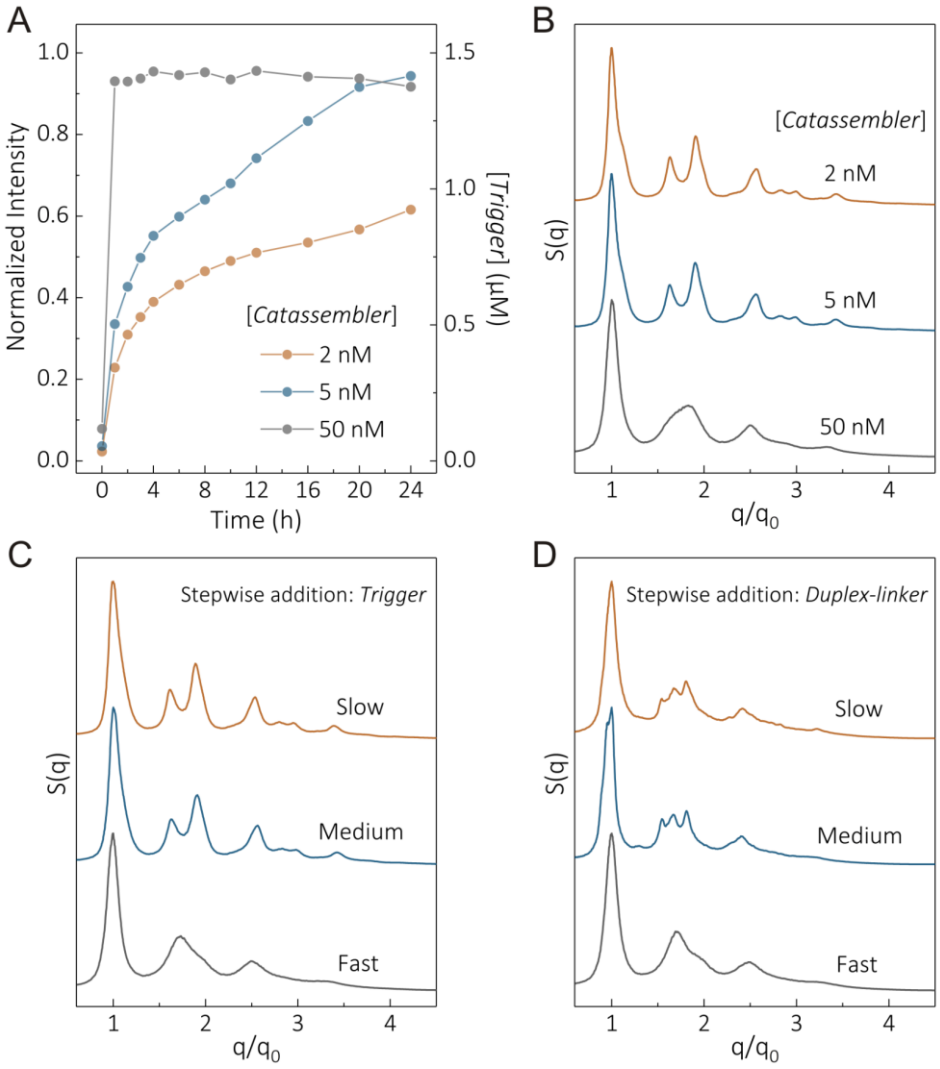

Fig. S13. (A) Fluorescence kinetic curves with the addition of different amounts of *Catassembler*. Here, [*Substrate*] = 1.5 μM, [*Fuel*] = 3 μM, and [*Reporter*] = 2 μM. (B) SAXS patterns of PAE aggregates with a DNA circuit-controlled release of *Trigger* driven by different amounts of *Catassembler*. Here, [*dPAE*] = 25 nM, [*Duplex-linker'*] = 750 nM, [*Substrate*] = 1.5 μM, and [*Fuel*] = 3 μM. (C) SAXS data of PAE aggregates obtained after the manual addition of *Trigger* into PAE assembly system according to the actual release amounts of *Trigger* marked in those fluorescence kinetic curves (slow, medium, and fast). Here, [*dPAE*] = 25 nM, [*Duplex-linker'*] = 750 nM. (D) SAXS measurements of PAE aggregates with the stepwise addition of *Duplex-linker* into the solution of DNA-AuNPs at different rates (slow, medium, and fast). Here, [*DNA-AuNP*] = 25 nM, and the final concentration of *Duplex-linker* in the assembly system was 750 nM.

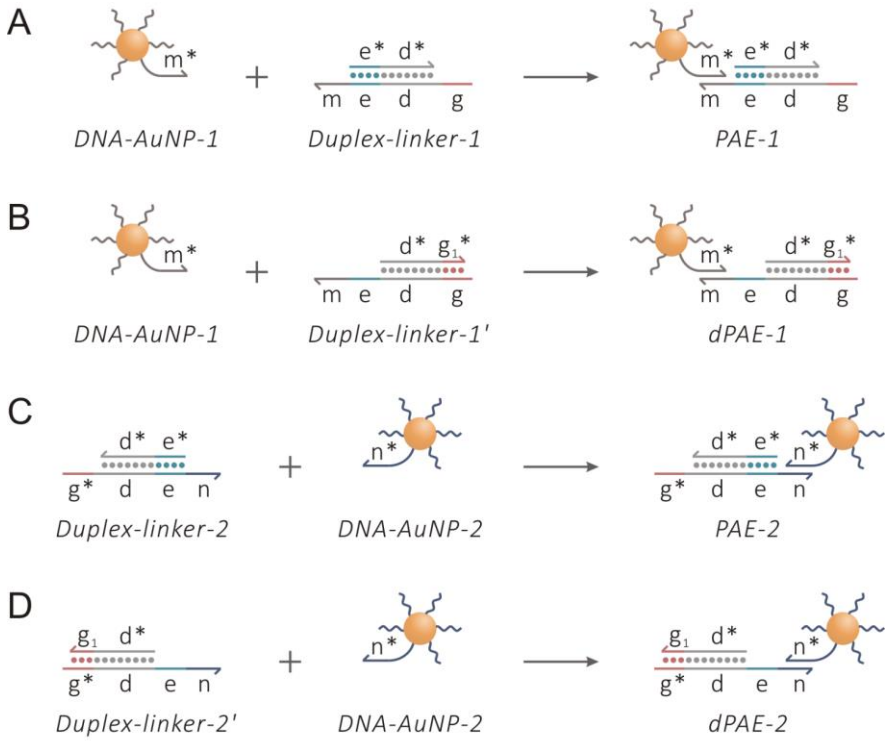

Fig. S14. Preparation process of the two types of PAEs (*PAE-1* and *PAE-2*) used for the thermal annealing strategy (A and C) and the two types of deactivated PAEs (*dPAE-1* and *dPAE-2*) used for the time-dependent interaction scheme (B and D) in the binary PAE assembly system.

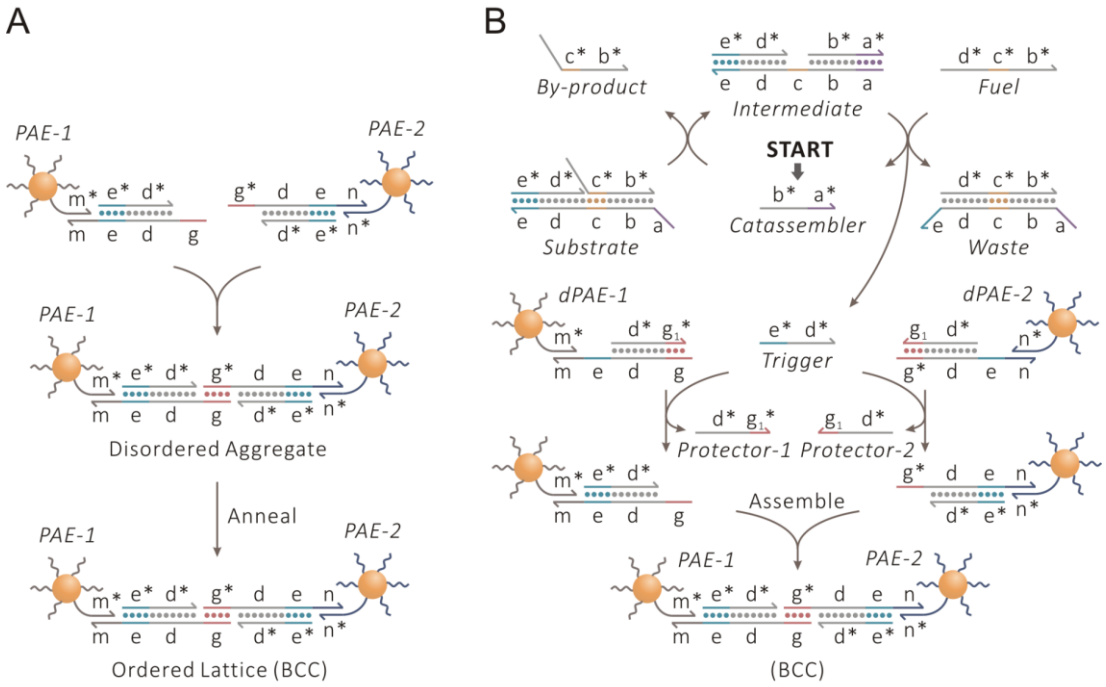

Fig. S15. (A) Scheme of PAE assembly in the binary system via the energy-invariant thermal annealing strategy. (B) Scheme of the PAE assembly process in the binary system using the time-dependent interaction strategy.

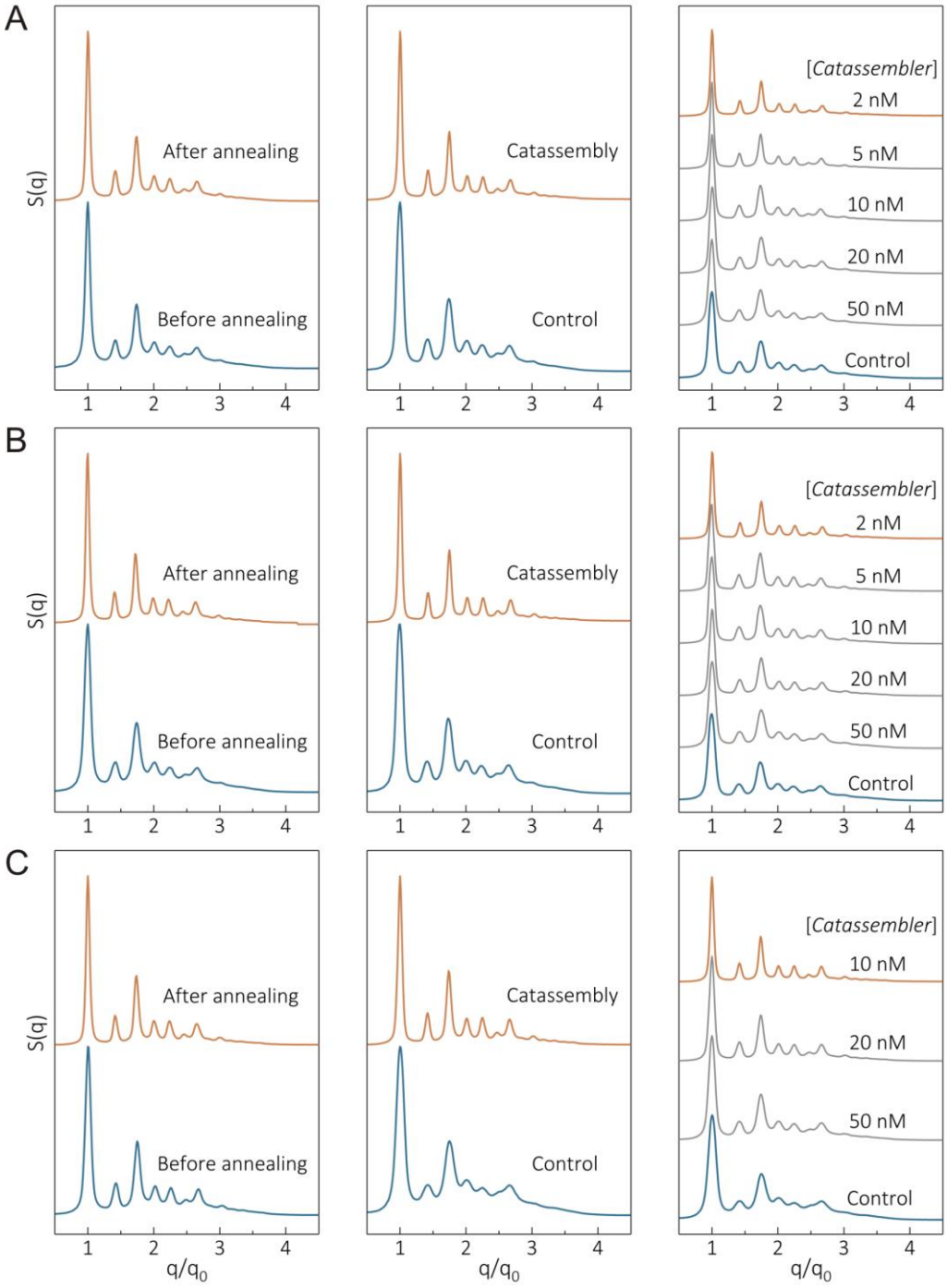
A
B
C
S(q)
After annealing
Before annealing
Catassembly
Control
[Catassembler]
2 nM
5 nM
10 nM
20 nM
50 nM
Control
1
2
3
4
q/q0

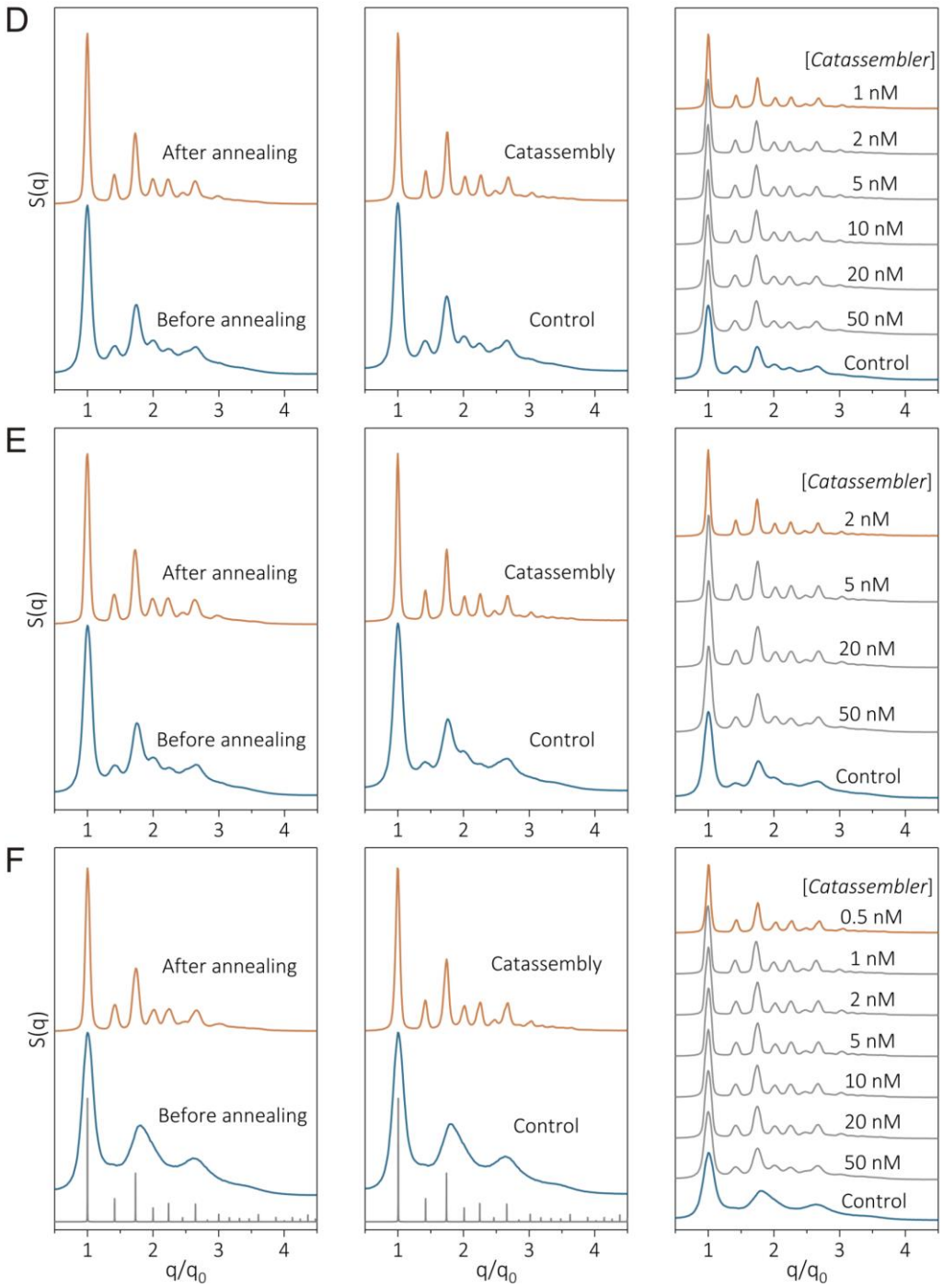

Fig. S16. SAXS patterns of the formed PAE aggregates in a binary system with linker/DNA-AuNP ratios of (A) 40:1, (B) 45:1, (C) 50:1, (D) 55:1, (E) 60:1, and (F) 80:1. From left to right, the panels represent 1D SAXS patterns for PAE aggregates formed via the thermal annealing strategy; SAXS patterns for PAE aggregates formed via the time-dependent interaction strategy; and SAXS patterns for PAE aggregates prepared with the addition of different amounts of *Catassembler*. The gray lines at the bottom of (F) represent theoretical X-ray scattering patterns for a perfect BCC lattice. Here, [*PAE-1*] = [*PAE-2*] = 12.5 nM in the thermal annealing strategy; for the time-dependent interaction scheme, [*dPAE-1*] = [*dPAE-2*] = 12.5 nM, [*Substrate*] = 2× ([*Duplex-linker-1'*] + [*Duplex-linker-2'*]), and [*Fuel*] = 2× [*Substrate*].

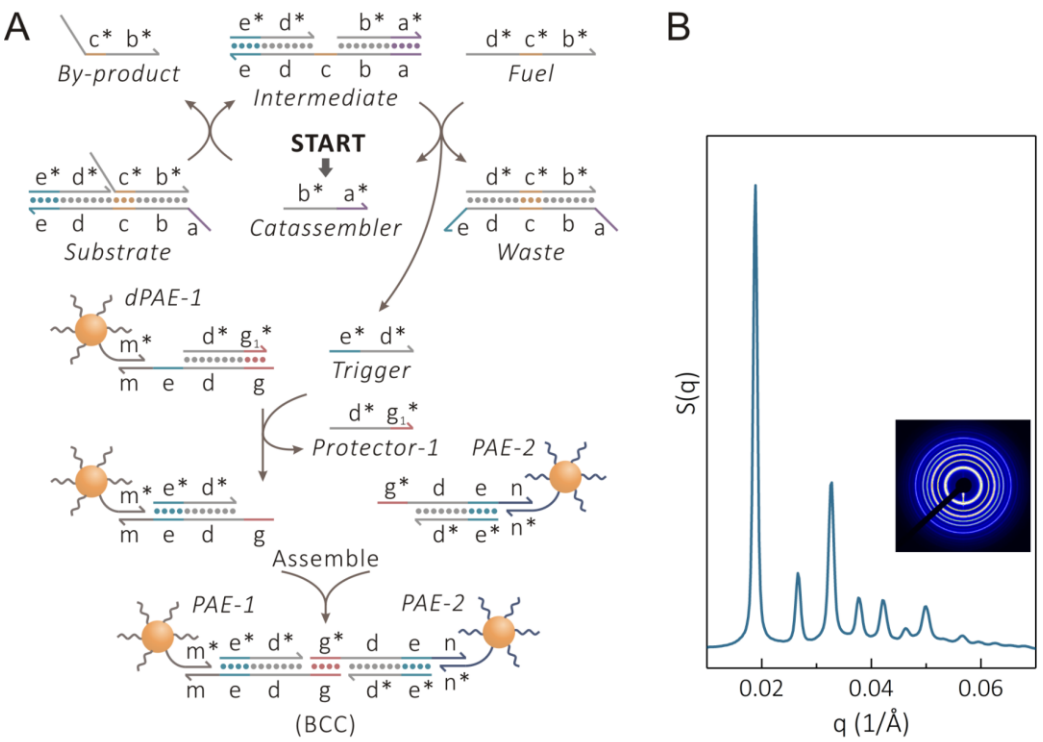

Fig. S17. (A) Scheme of PAE assembly in the binary system based on the time-dependent interaction scheme, where the architecture of *dPAE-1* has protected sticky ends and *PAE-2* has active sticky ends. (B) 1D and 2D SAXS patterns of PAE aggregates prepared using the modified strategy. Here, *dPAE-1* and *PAE-2* were prepared by hybridizing two kinds of duplex linkers to each PAE at a ratio of 50:1. In this experiment, [*dPAE-1*] = [*PAE-2*] = 12.5 nM, [*Substrate*] = 1.25 μM, [*Fuel*] = 2.5 μM, and [*Catassembler*] = 2 nM.

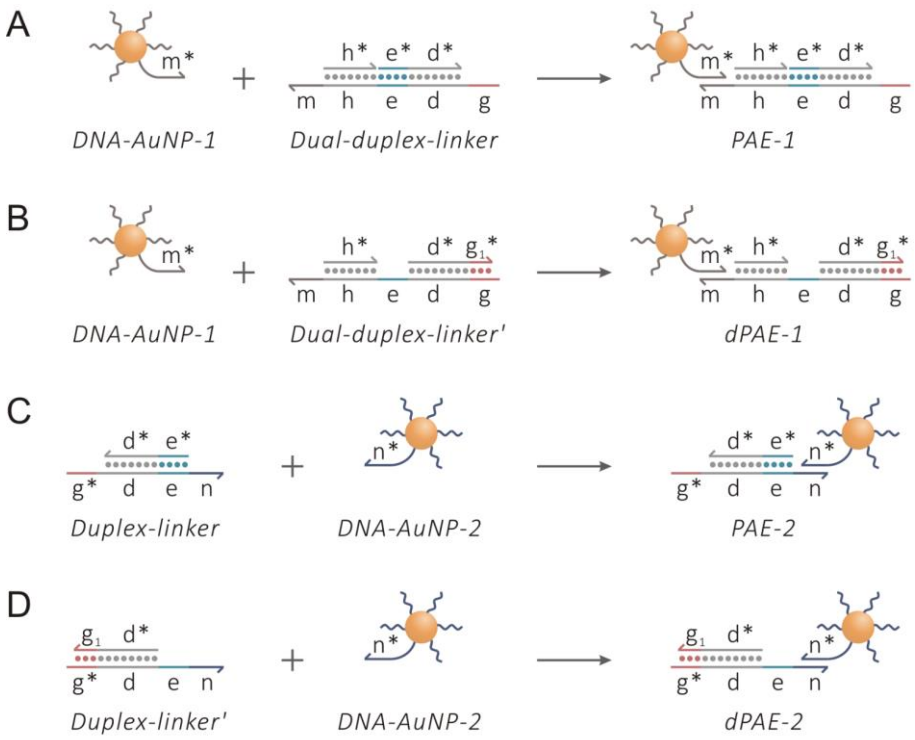

Fig. S18. (A-D) Scheme for the preparation of two types of PAEs (*PAE-1* and *PAE-2*) with active sticky ends and their derivatives (*dPAE-1* and *dPAE-2*) with protected sticky ends used in asymmetric binary systems.

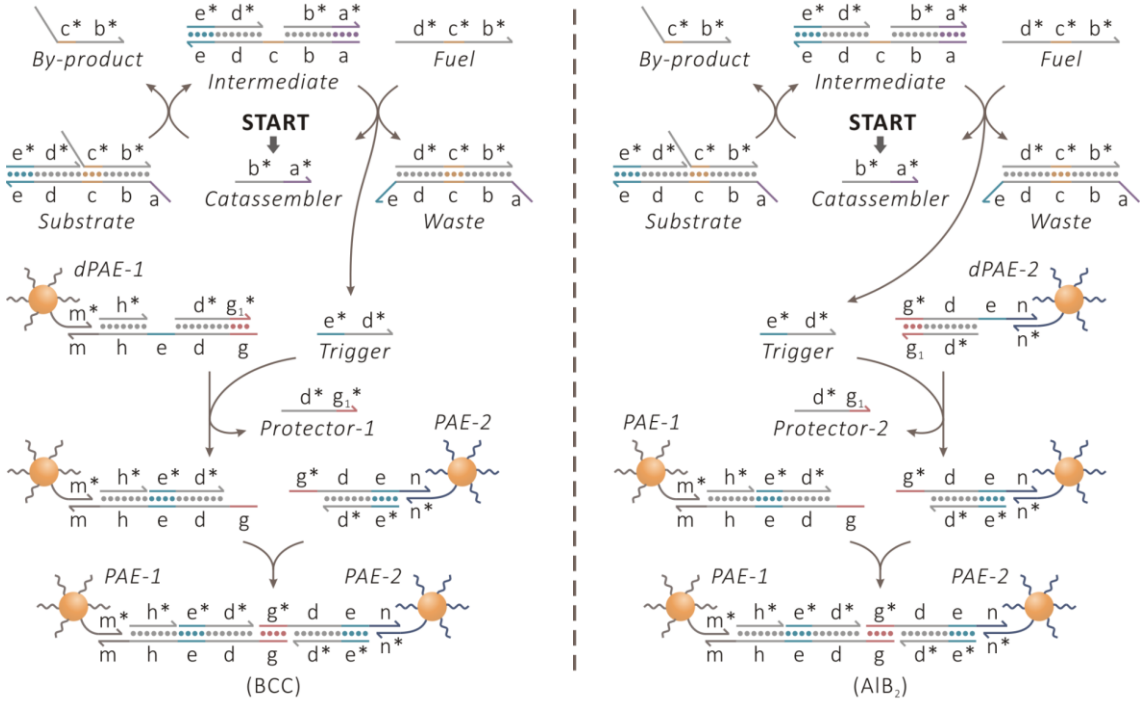

Fig. S19. Schematic representation of PAE crystallization in two asymmetric binary systems programmed by the same DNA strand-displacement circuit independently.

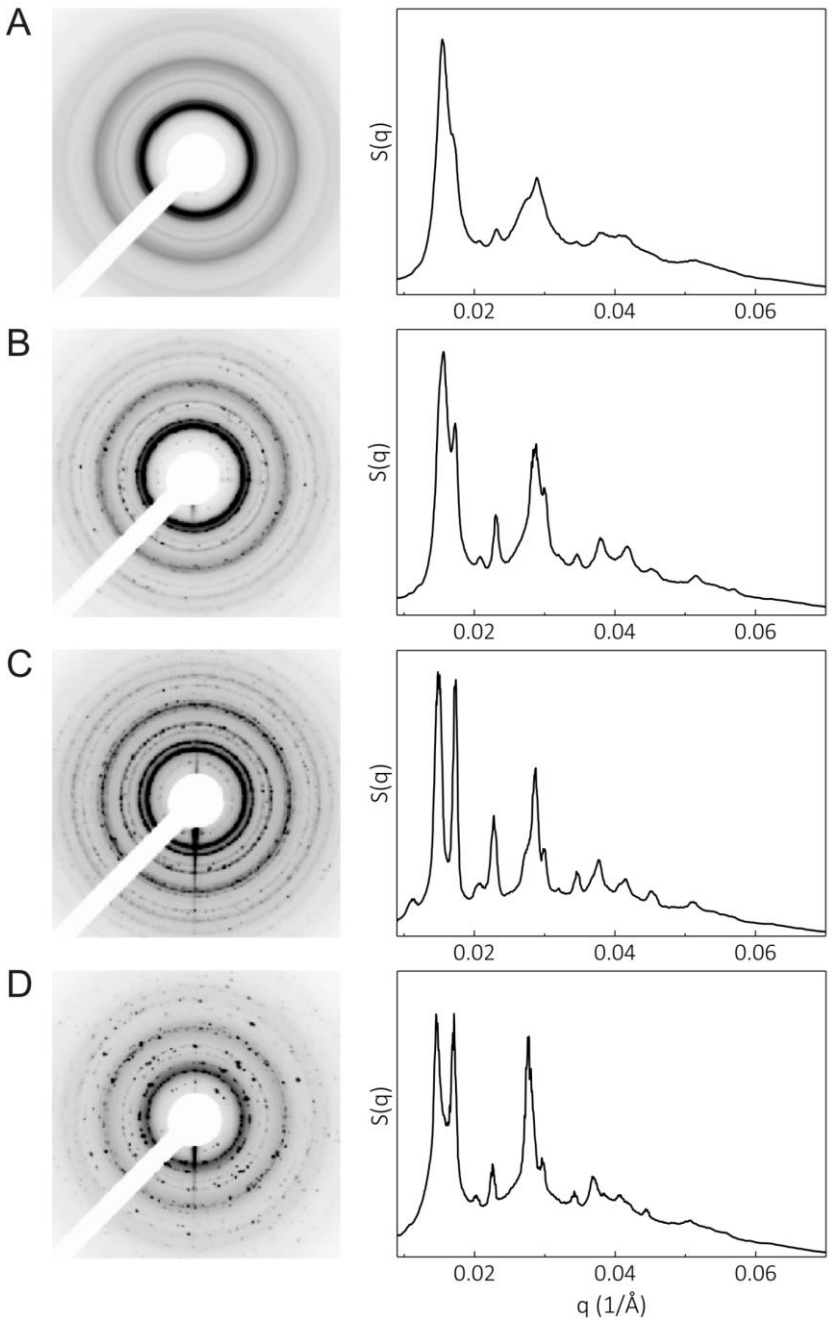

Fig. S20. 2D and 1D SAXS data for PAE aggregates prepared with *Catassembler* concentrations of (A) 50 nM, (B) 5 nM, (C) 2 nM, and (D) 1 nM added to the asymmetric binary system containing *PAE-1 and dPAE-2*. The AlB_2 lattice gradually formed as the amount of *Catassembler* added decreased. Individual scattering spots in 2D SAXS patterns represent the formation of large crystalline domains of AlB_2 structures. Here, the numbers of DNA linkers on *PAE-1* and *dPAE-2* were 80 and 40, respectively. [*PAE-1*] = 6 nM, [*dPAE-2*] = 24 nM, [*Substrate*] = 1.92 μM, and [*Fuel*] = 3.84 μM.

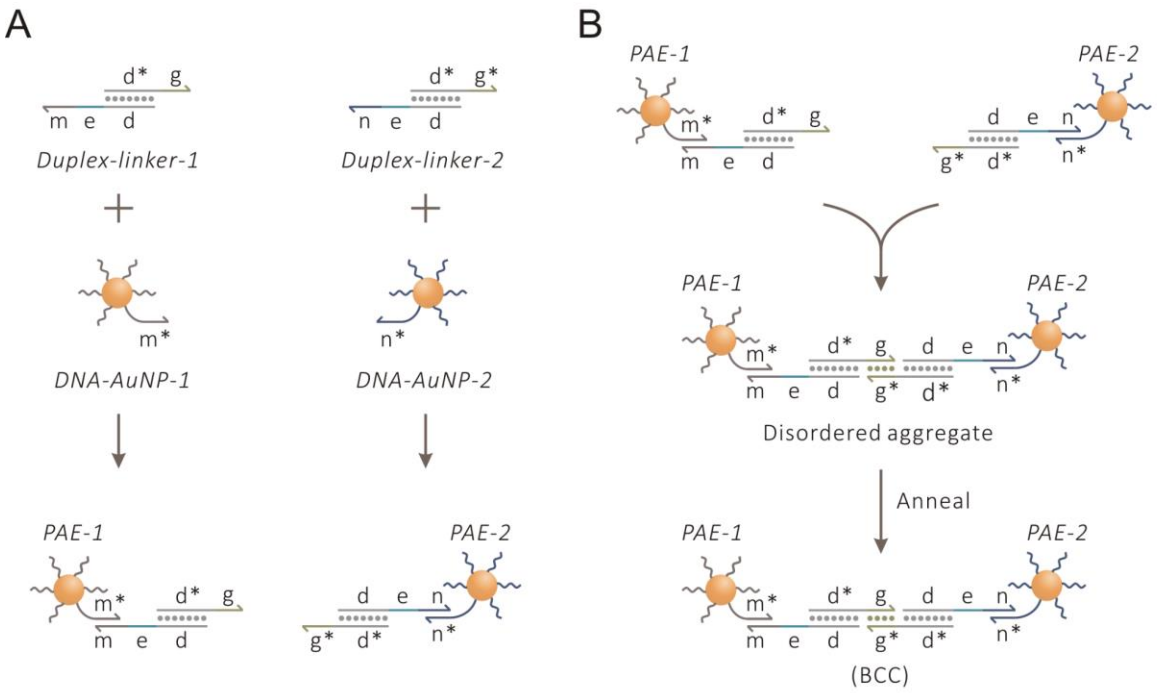

Fig. S21. Graphical representation of the formation processes of *PAE-1* and *PAE-2* (A) and the corresponding PAE assembly process via thermal annealing (B), where *PAE-1* has a non-self-complementary sticky end of $^{5'}$–AAGGAA$^{3'}$ (domain g) and *PAE-2* has a non-self-complementary sticky end of $^{5'}$–TTCCTT$^{3'}$ (domain g*). The prepared BCC lattices can be dynamically converted into FCC lattices programmed by a DNA circuit as described in section S2.9.

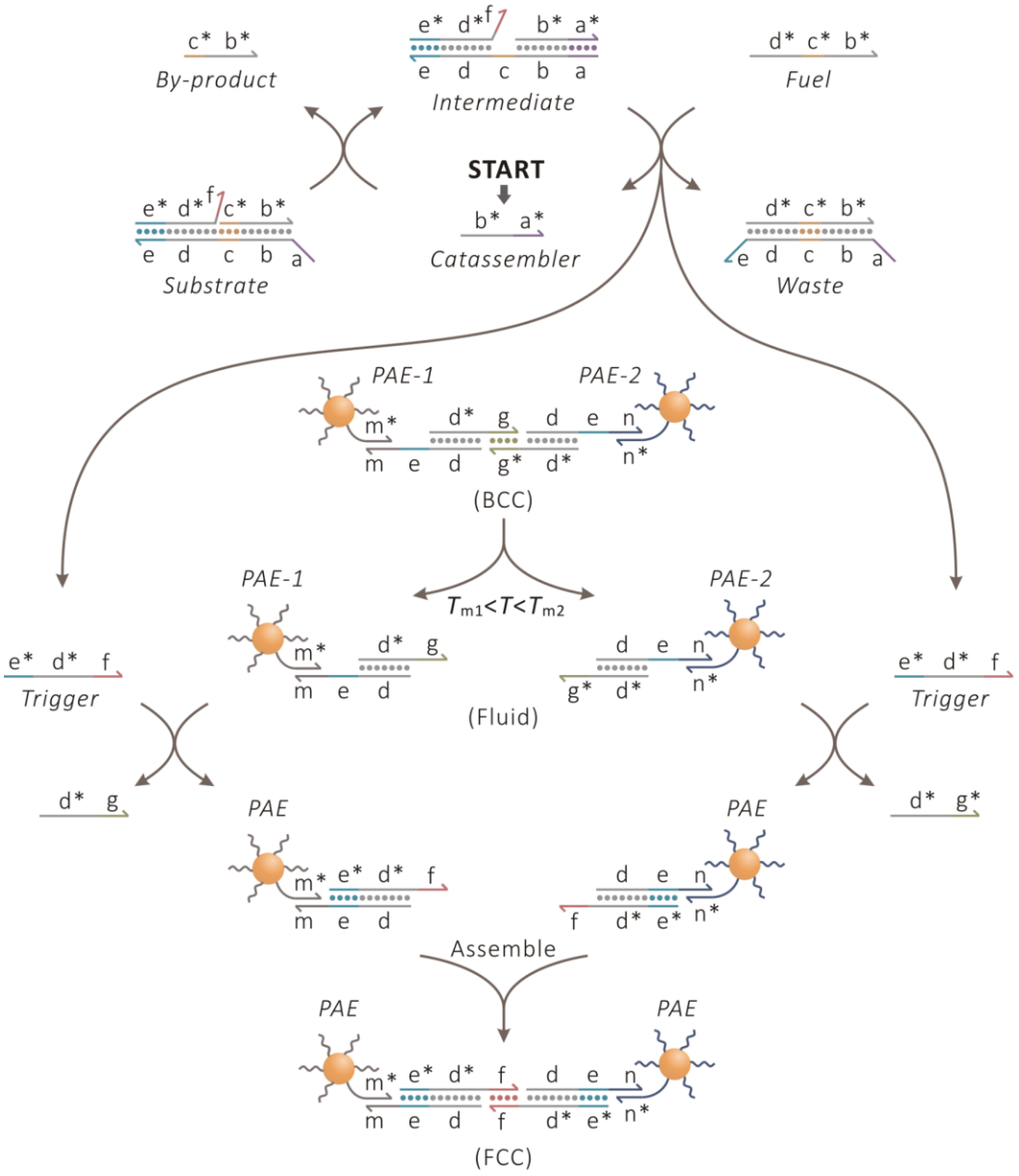

Fig. S22. A detailed scheme showing how a binary system having a pair of non-self-complementary sticky ends of $^{5'}$−AAGGAA$^{3'}$ and $^{5'}$−TTCCTT$^{3'}$ on *PAE-1* and *PAE-2*, respectively, is dynamically converted into a unary system having a self-complementary sticky end of $^{5'}$−TGCGCA$^{3'}$ on all PAEs (*PAE*) under programming by a time-dependent DNA strand-displacement circuit at a temperature between the melting points of the two PAE systems ($T_{m1} < T < T_{m2}$).

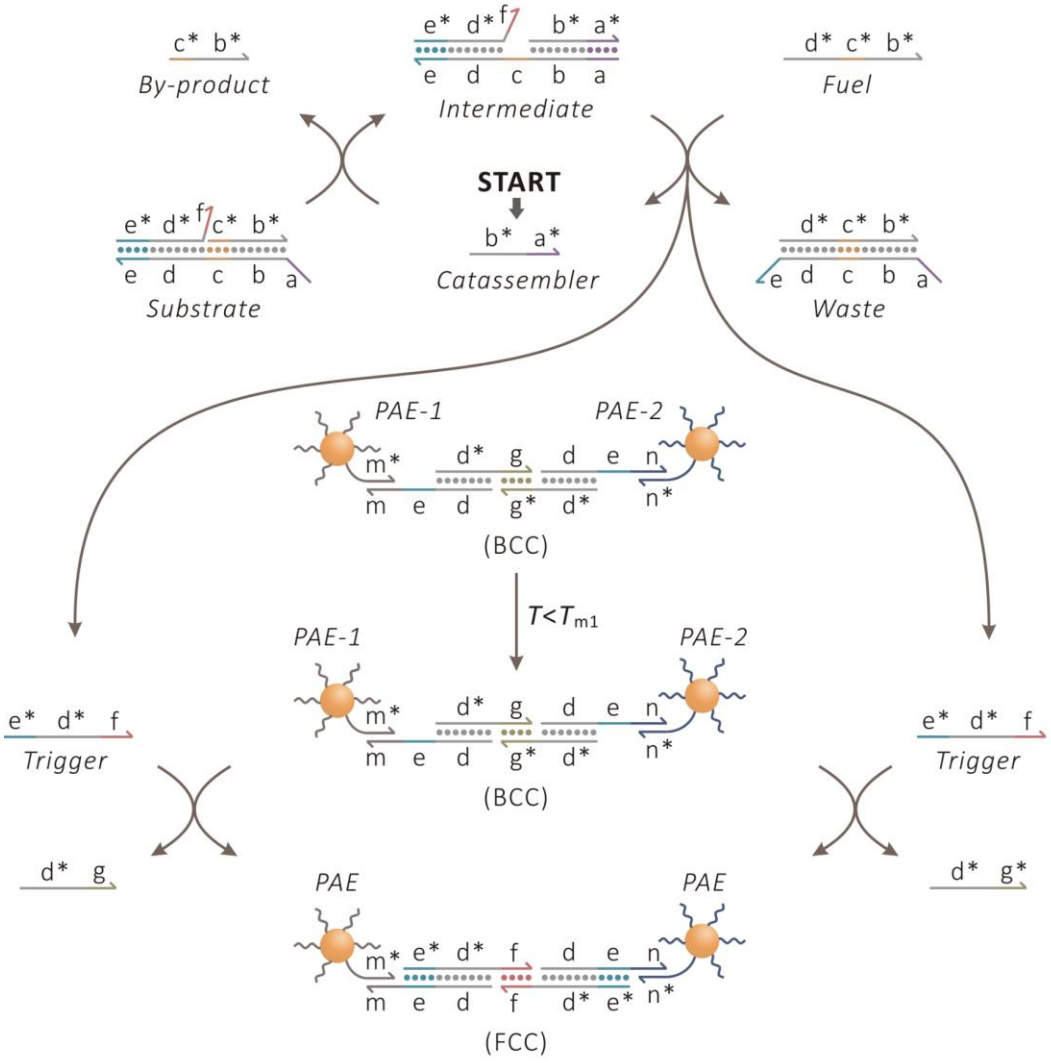

Fig. S23. A detailed scheme showing how a binary system having a pair of non-self-complementary sticky ends of $^{5'}$−AAGGAA$^{3'}$ and $^{5'}$−TTCCTT$^{3'}$ on *PAE-1* and *PAE-2*, respectively, is dynamically converted into a unary system having a self-complementary sticky end of $^{5'}$−TGCGCA$^{3'}$ on all PAEs (*PAE*) under programming by a time-dependent DNA strand-displacement circuit at temperatures lower than the melting point of the binary system ($T < T_{m1}$).

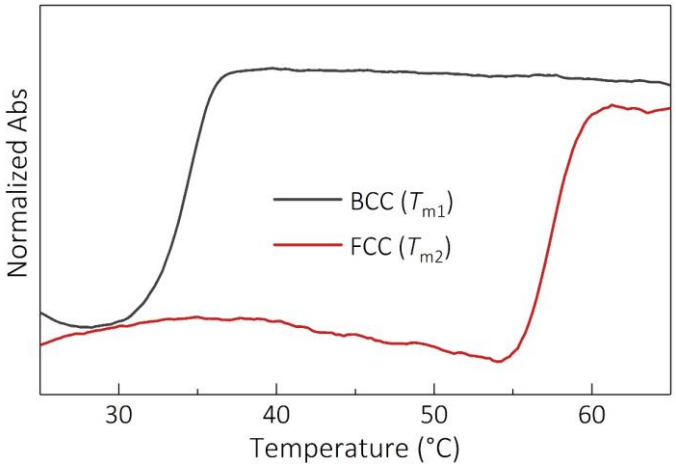

Fig. S24. The melting curves of the BCC lattice before the dynamic lattice transformation shown in Fig. 3A (black line: T_{m1} ~34 ℃) and the FCC lattice after the dynamic lattice transformation shown in Fig. 3A (red line: T_{m2} ~57 ℃).

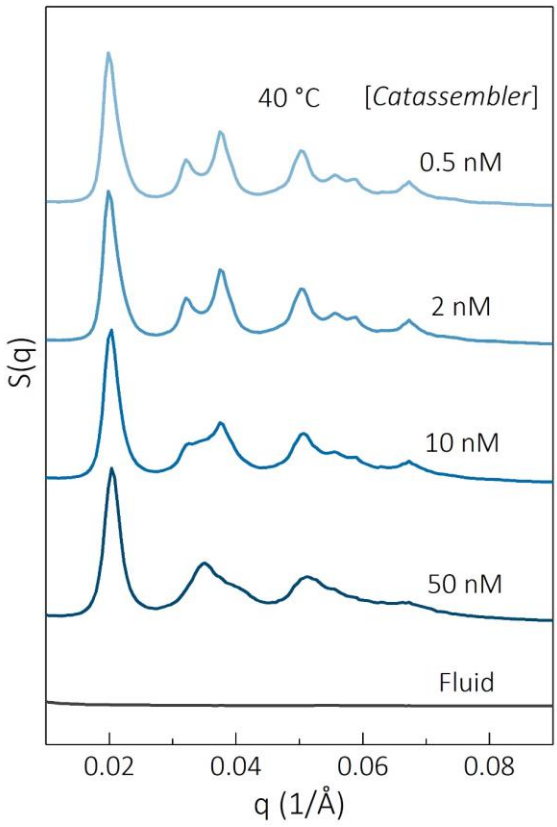

Fig. S25. The SAXS test results of the transformation of PAE lattice from BCC to FCC after the addition of different concentrations of *Catassembler* at 40 ℃. A unary FCC lattice was formed in the presence of lower concentrations of *Catassembler* (0.5 and 2 nM) under programming of the DNA strand-displacement circuit. Since the reaction temperature of 40 ℃ was higher than the melting temperature of the binary system (~34 ℃), the structural transformation occurred from the BCC phase to a fluid phase and then to the FCC phase. Here, [*PAE-1*] = [*PAE-2*] = 12.5 nM, [*Duplex-linker-1*] = [*Duplex-linker-2*] = 500 nM, [*Substrate*] = 1.5 μM, and [*Fuel*] = 3 μM.

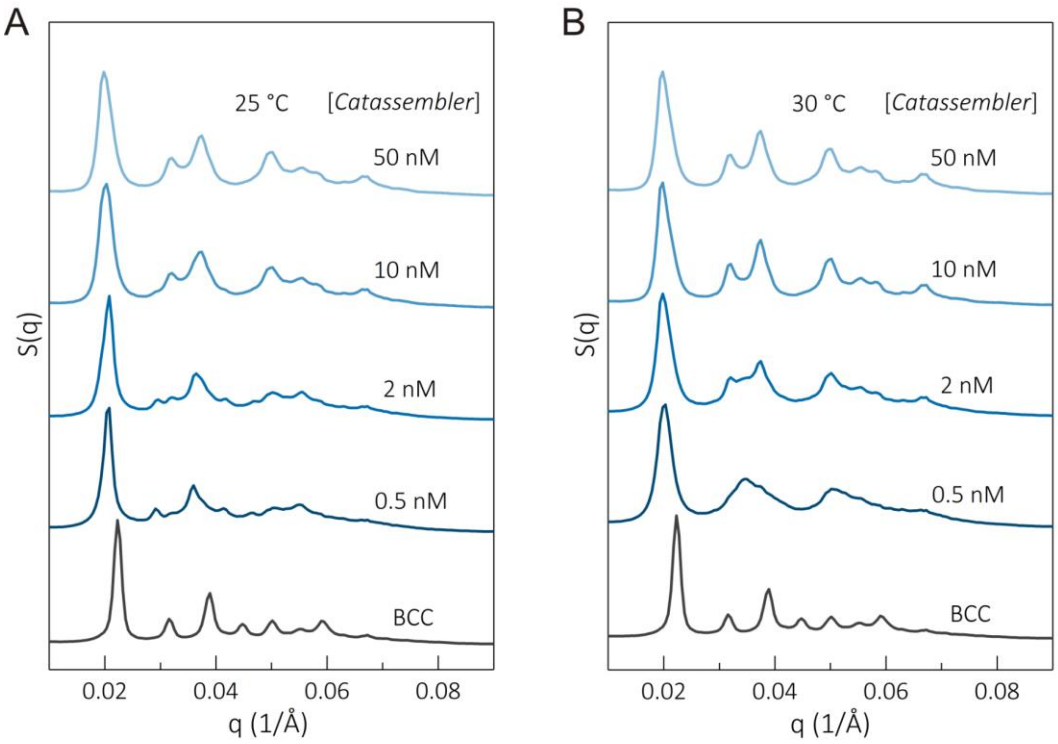

Fig. S26. The SAXS measurements of the transformation of PAE lattice from BCC to FCC after the addition of different concentrations of *Catassembler* at (A) 25 ℃ and (B) 30 ℃. A new unary FCC phase can be obtained from the initial binary BCC phase in the presence of higher concentrations of *Catassembler* (10 and 50 nM). Since the reaction temperature of 25 ℃ or 30 ℃ was lower than the melting temperature of the binary system (~34 ℃), the direct phase transition from BCC FCC occurred in a solid-solid manner. Here, [*PAE-1*] = [*PAE-2*] = 12.5 nM, [*Duplex-linker-1*] = [*Duplex-linker-2*] = 500 nM, [*Substrate*] = 1.5 μM, and [*Fuel*] = 3 μM.

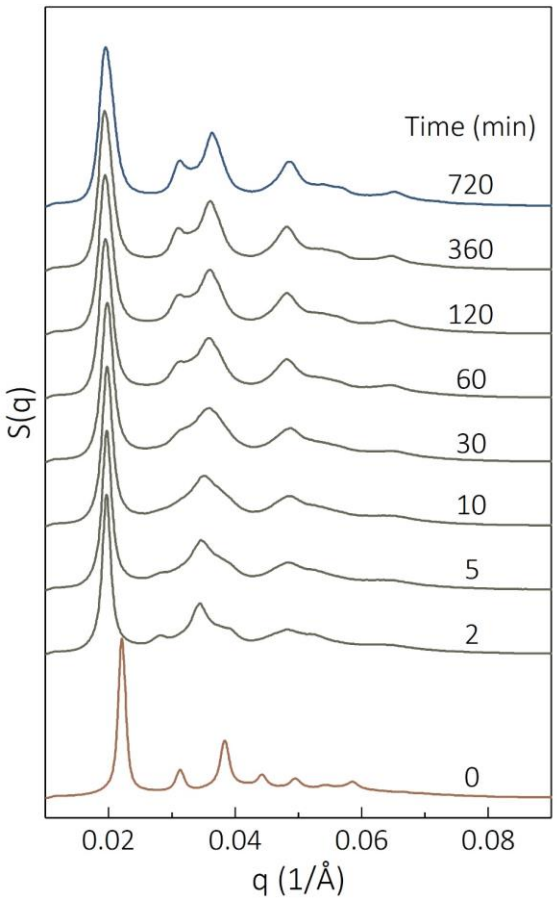

Fig. S27. The time evolution of the *in situ* SAXS-measured structure factor, S(q), of the binary BCC structure in the presence 1.5 μM *Trigger* at 25 ℃**.** A new unary FCC phase was gradually developed from the initial binary BCC phase with the increase of time in a solid-solid transition manner.

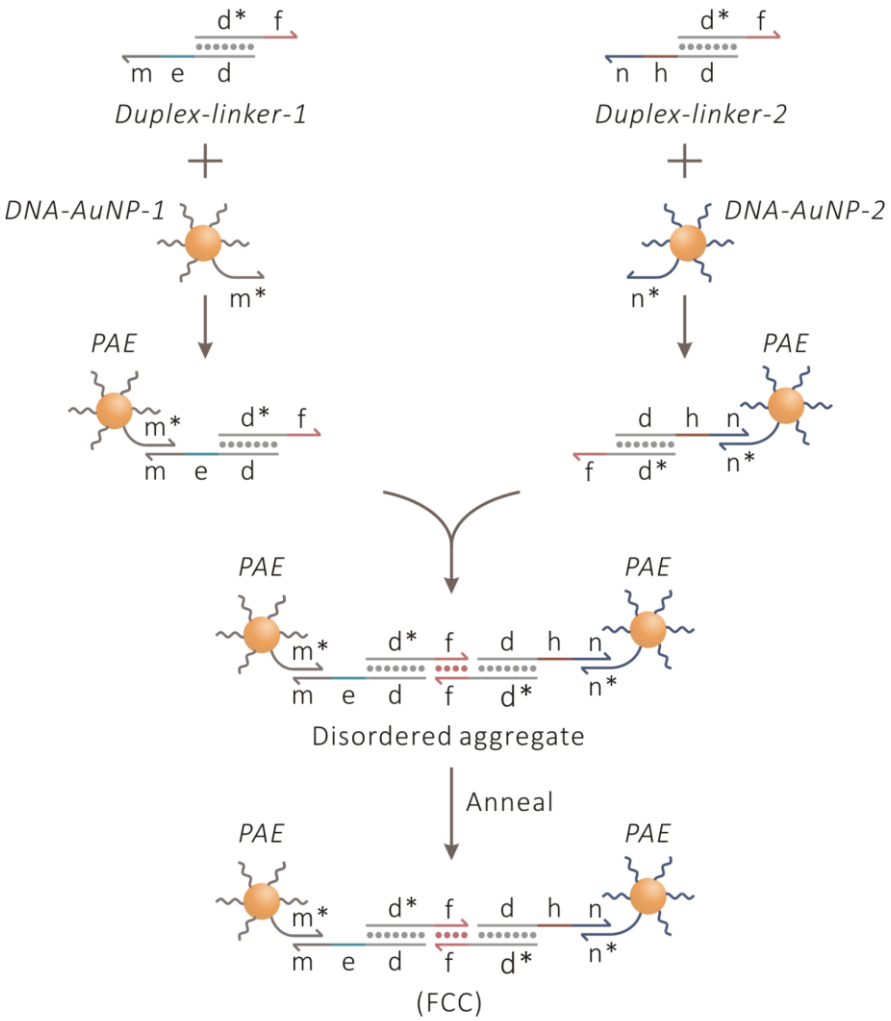

Fig. S28. Graphical representation of the formation process of the unary FCC structure upon thermal annealing treatment, where all PAEs have a self-complementary sticky end of $^{5'}$−TAGCTA$^{3'}$ (domain f). The prepared unary FCC lattices can be dynamically converted into binary BCC lattices programmed by two DNA circuits as described in section S2.10.

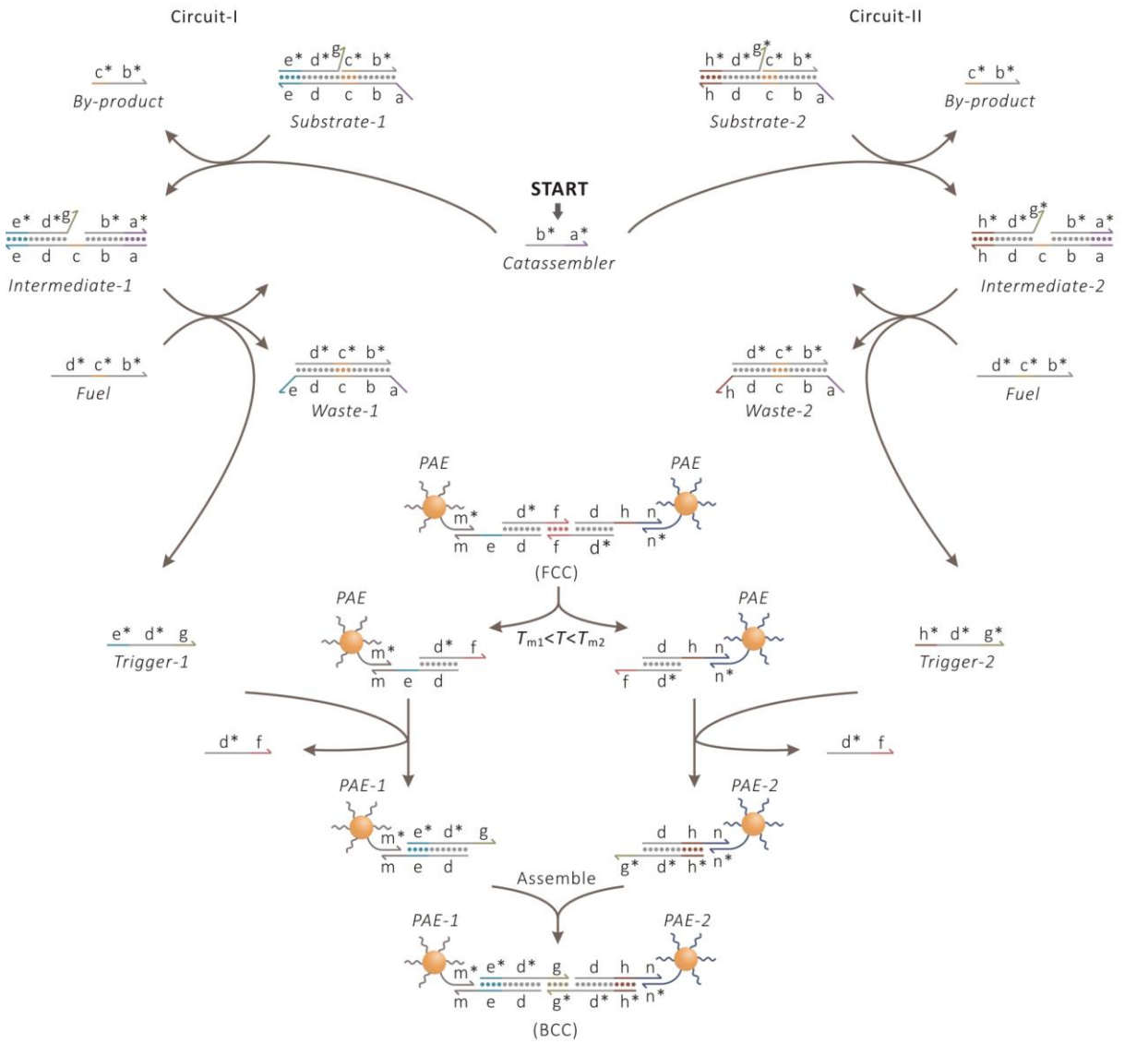

Fig. S29. A detailed scheme showing how a unary PAE system (T_{m1} ~37 °C) having a self-complementary sticky end of $^{5'}$-TAGCTA$^{3'}$ on all PAEs (*PAE*) is dynamically converted into a binary PAE system (T_{m2} ~51 °C) having a pair of non-self-complementary sticky ends of $^{5'}$-GGAAGG$^{3'}$ and $^{5'}$-CCTTCC$^{3'}$ on *PAE-1* and *PAE-2* under control of two parallel catassembly DNA strand-displacement circuits.

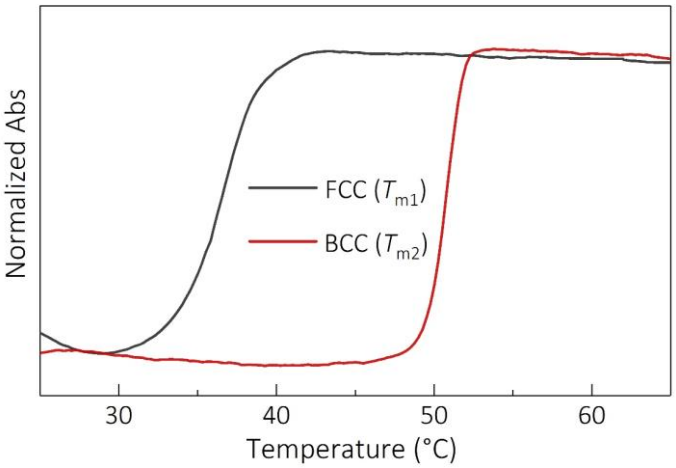

Fig. S30. The melting curves of the FCC lattice before the dynamic lattice transformation shown in Fig. 3C (black line: T_{m1} ~37 ℃) and the BCC lattice after the dynamic lattice transformation shown in Fig. 3C (red line: T_{m2} ~51℃).

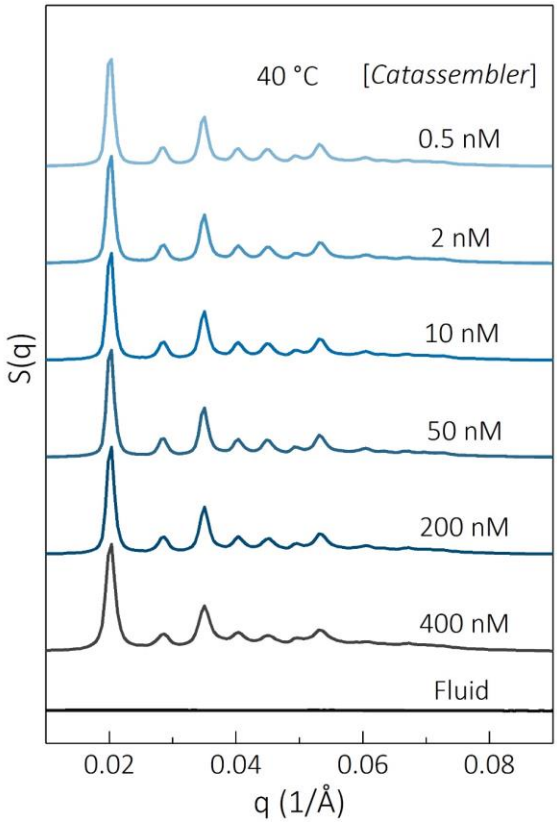

Fig. S31. The SAXS measurements of the transformation of PAE lattice from FCC to BCC at 40 ℃. A binary BCC structure can be formed with the addition of different concentrations of the input *Catassembler* (from 400 to 0.5 nM) driven by two DNA strand-displacement circuits. Since the reaction temperature of 40 ℃ was higher than the melting temperature of the initial unary FCC system (37 ℃), the structural transformation occurred from the initial FCC phase to a fluid phase and then to the BCC phase. Here, [*PAE*] = 25 nM, [*Duplex-linker-1*] = [*Duplex-linker-2*] = 500 nM, [*Substrate-1*] = [*Substrate-2*] = 750 nM, and [*Fuel*] = 3 μM.

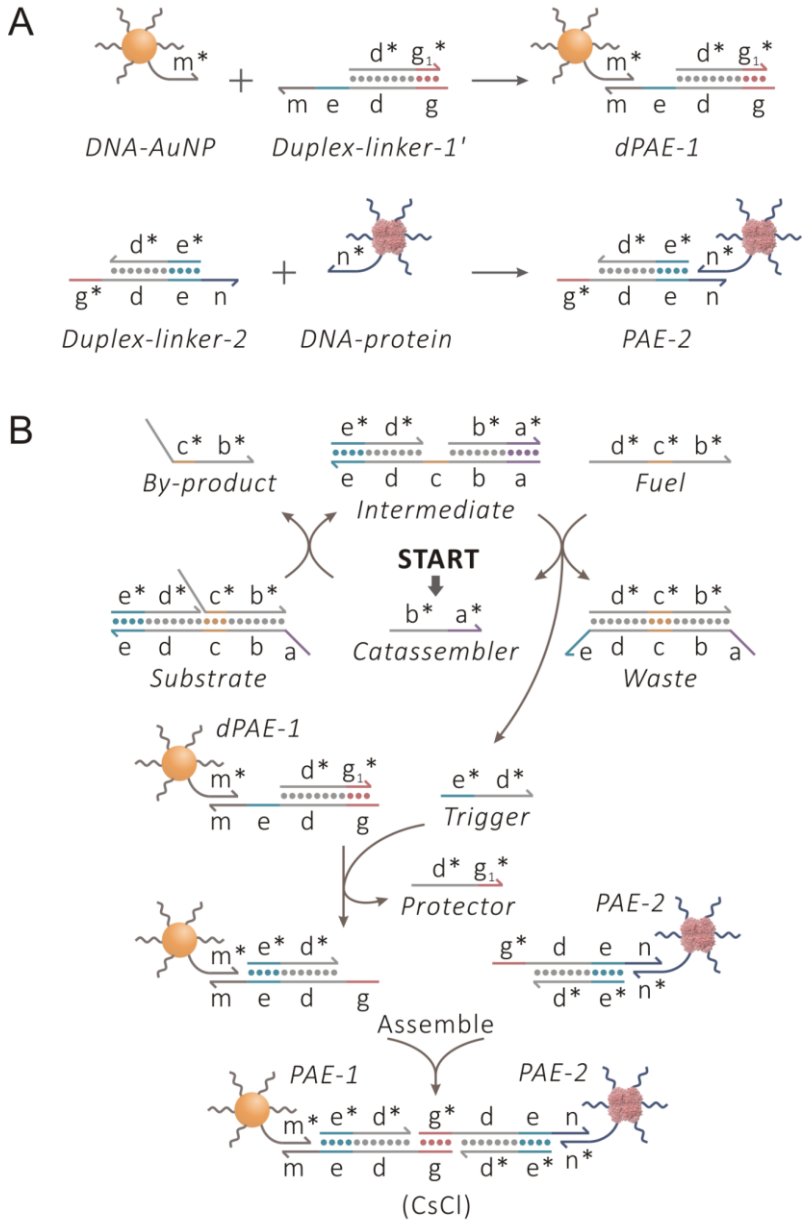

Fig. S32. (A) Schematic representation of the preparation of *dPAE-1* (formed through the hybridization of *DNA-AuNP* and *Duplex-linker-1'*) and *PAE-2* (formed through the hybridization of *DNA-protein* and *Duplex-linker-2*) used in the binary AuNP-protein assembly system. (B) Scheme for the assembly process of the binary AuNP-protein system driven by the DNA circuit.

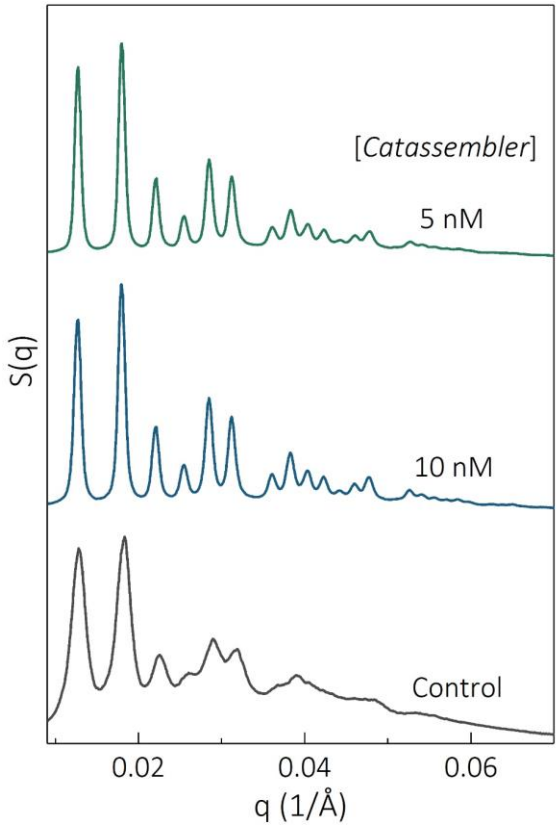

Fig. S33. SAXS patterns of PAE lattices for the binary AuNP-protein system. Well-ordered CsCl lattices composed of AuNPs and proteins were obtained by controlling *Trigger* release through the addition of 5 nM and 10 nM *Catassembler* using the time-dependent interaction strategy, as demonstrated by the exhibited simple cubic scattering patterns, since, relative to that of the AuNPs, the scattering of the proteins in the practical SAXS measurements was negligible. In comparison, the direct addition of a full amount of *Trigger* strand (2.4 μM) resulted in a poorly ordered crystal (shown in the "Control" curve). Here, [*dPAE-1*] = [*PAE-2*] = 15 nM, [*Duplex-linker-1'*] = [*Duplex-linker-2*] = 1.2 μM, [*Substrate*] = 2.4 μM, and [*Fuel*] = 4.8 μM, where *dPAE-1* denotes the DNA-AuNP conjugate and *PAE-2* denotes the DNA-protein conjugate.

S4. Supplementary Tables

Table S1. The DNA sequences used in the unary PAE assembly systems (Fig. 1 and Figs. S6-S13).

Name	Domains (5' to 3')	Sequences (5' to 3')
Bottom-substrate	a-b-c-d-e	TGAAGG_GCGAGTATGATATGGC_AGGG_CGGTAAGT TAGTTGAG_GATCTG
By-product	c*-b*	TTTTTTTTTTTTTTT_CCCT_GCCATATCATACTCGC
Trigger	e*-d*	CAGATC_CTCAACTAACTTACCG
Fuel	d*-c*-b*	CTCAACTAACTTACCG_CCCT_GCCATATCATACTCGC
Catassembler	b*-a*	GCCATATCATACTCGC_CCTTCA
AuNP-SH	m*	HS-AAAAAAAAAA_AAGACGAATATTTAACAA
Linker	f-d-e-m	CGCG_A_CGGTAAGTTAGTTGAG_GATCTG_A_TTGTT AAATATTCGTCTT
Protector	d*-f_1*	CTCAACTAACTTACCG_T_CGC

Table S2. The DNA sequences used in the binary PAE assembly systems (Figs. S14-S17).

Name	Domains (5' to 3')	Sequences (5' to 3')
Bottom-substrate	a-b-c-d-e	TGAAGG_GCGAGTATGATATGGC_AGGG_CGGTAAGT TAGTTGAG_GATCTG
By-product	c*-b*	TTTTTTTTTTTTTTT_CCCT_GCCATATCATACTCGC
Trigger	e*-d*	CAGATC_CTCAACTAACTTACCG
Fuel	d*-c*-b*	CTCAACTAACTTACCG_CCCT_GCCATATCATACTCGC
Catassembler	b*-a*	GCCATATCATACTCGC_CCTTCA
AuNP-SH 1	m*	HS-AAAAAAAAAA_AACGACTCATATTAAGAA
AuNP-SH 2	n*	HS-AAAAAAAAAA_AAGACGAATATTTAACAA
Linker-1	g-d-e-m	TTCCTT_A_CGGTAAGTTAGTTGAG_GATCTG_A_TTCT TAATATGAGTCGTT
Linker-2	g*-d-e-n	AAGGAA_A_CGGTAAGTTAGTTGAG_GATCTG_A_TTG TTAAATATTCGTCTT
Protector-1	d*-g_1*	TCAACTAACTTACCG_T_AAG
Protector-2	d*-g_1	TCAACTAACTTACCG_T_TTC

Table S3. The DNA sequences used in the asymmetric binary PAE assembly systems (Fig. 2 and Figs. S18-S20).

Name	Domains (5' to 3')	Sequences (5' to 3')
Bottom-substrate	a-b-c-d-e	TGAAGG_GCGAGTATGATATGGC_AGGG_CGGTAAGT TAGTTGAG_GATCTG
By-product	c*-b*	TTTTTTTTTTTTTTT_CCCT_GCCATATCATACTCGC
Trigger	e*-d*	CAGATC_CTCAACTAACTTACCG
Fuel	d*-c*-b*	CTCAACTAACTTACCG_CCCT_GCCATATCATACTCGC
Catassembler	b*-a*	GCCATATCATACTCGC_CCTTCA
AuNP-SH 1	m*	HS-AAAAAAAAAA_AACGACTCATATTAAGAA
AuNP-SH 2	n*	HS-AAAAAAAAAA_AAGACGAATATTTAACAA
Linker-1	g-d-e-h-m	TTCCTT_A_CGGTAAGTTAGTTGAG_GATCTG_TTTTTT TTTTTTTTTTTTTTTTTTT_A_TTCTTAATATGAGTCGT T
Linker-2	g*-d-e-n	AAGGAA_A_CGGTAAGTTAGTTGAG_GATCTG_A_TTG TTAAATATTCGTCTT
Protector-1	d*-g_1*	TCAACTAACTTACCG_T_AAG
Protector-2	d*-g_1	TCAACTAACTTACCG_T_TTC
Duplexer	h*	AAAAAAAAAAAAAAAAAAAAAAAAA

Table S4. The DNA sequences used in the experiments on the structural transformation of the PAE lattice from BCC to FCC (Fig. 3A and Figs. S21-S27).

Name	Domains (5' to 3')	Sequences (5' to 3')
Bottom-substrate	a-b-c-d-e	TGAAGG_GCGAGTATGATATGGC_AGGG_CGGTAAGT TAGTTGAG_GATCTG
By-product	c*-b*	CCCT_GCCATATCATACTCGC
Trigger	e*-d*-f	CAGATC_CTCAACTAACTTACCG_A_TGCGCA
Fuel	d*-c*-b*	CTCAACTAACTTACCG_CCCT_GCCATATCATACTCGC
Catassembler	b*-a*	GCCATATCATACTCGC_CCTTCA
AuNP-SH 1	m*	HS-AAAAAAAAAA_AAGACGAATATTTAACAA
AuNP-SH 2	n*	HS-AAAAAAAAAA_AACGACTCATATTAAGAA
h-AuNP-1	d-e-m	CGGTAAGTTAGTTGAG_GATCTG_A_TTGTTAAATATT CGTCTT
h-AuNP-2	d-e-n	CGGTAAGTTAGTTGAG_GATCTG_A_TTCTTAATATGA GTCGTT
p-AuNP-1	d*-g	CTCAACTAACTTACCG_A_AAGGAA
p-AuNP-2	d*-g*	CTCAACTAACTTACCG_A_TTCCTT

Table S5. The DNA sequences used in the experiments on the structural transformation of the PAE lattice from FCC to BCC (Fig. 3C and Figs. S28-S31).

Name	Domains (5' to 3')	Sequences (5' to 3')
Bottom-substrate-1	a-b-c-d-e	TGAAGG_GCGAGTATGATATGGC_AGGG_CGGTAAGTTAGTTGAG_GATCTG
Bottom-substrate-2	a-b-c-d-h	TGAAGG_GCGAGTATGATATGGC_AGGG_CGGTAAGTTAGTTGAG_GTCTAG
By-product	c*-b*	CCCT_GCCATATCATACTCGC
Trigger-1	e*-d*-g	CAGATC_CTCAACTAACTTACCG_A_GGAAGG
Trigger-2	h*-d*-g*	CTAGAC_CTCAACTAACTTACCG_A_CCTTCC
Fuel	d*-c*-b*	CTCAACTAACTTACCG_CCCT_GCCATATCATACTCGC
Catassembler	b*-a*	GCCATATCATACTCGC_CCTTCA
AuNP-SH 1	m*	HS-AAAAAAAAAA_AAGACGAATATTTAACAA
AuNP-SH 2	n*	HS-AAAAAAAAAA_AACGACTCATATTAAGAA
h-AuNP-1	d-e-m	CGGTAAGTTAGTTGAG_GATCTG_A_TTGTTAAATATTCGTCTT
h-AuNP-2	d-h-n	CGGTAAGTTAGTTGAG_GTCTAG_A_TTCTTAATATGAGTCGTT
p-AuNP	d*-f	CTCAACTAACTTACCG_A_TAGCTA

Table S6. The DNA sequences used in the binary AuNP-protein assembly system (Fig. 4 and Figs. S32 and S33).

Name	Domains (5' to 3')	Sequences (5' to 3')
Bottom-substrate	a-b-c-d-e	TGAAGG_GCGAGTATGATATGGC_AGGG_CGGTAAG TTAGTTGAG_GATCTG
By-product	c*-b*	TTTTTTTTTTTTTTT_CCCT_GCCATATCATACTCGC
Trigger	e*-d*	CAGATC_CTCAACTAACTTACCG
Fuel	d*-c*-b*	CTCAACTAACTTACCG_CCCT_GCCATATCATACTCG C
Catassembler	b*-a*	GCCATATCATACTCGC_CCTTCA
AuNP-SH	m*	HS-AAAAAAAAAA_AACGACTCATATTAAGAA
protein-DBCO	n*	DBCO-AAAAAAAAAA_AAGACGAATATTTAACAA
Linker-1	g-d-e-m	TTCCTT_A_CGGTAAGTTAGTTGAG_GATCTG_A_TTC TTAATATGAGTCGTT
Linker-2	g*-d-e-n	AAGGAA_A_CGGTAAGTTAGTTGAG_GATCTG_A_TT GTTAAATATTCGTCTT
Protector	d*-g_1*	TCAACTAACTTACCG_T_AAG

S5. References

1. J. N. Zadeh *et al.*, NUPACK: Analysis and design of nucleic acid systems. *J. Comput. Chem.* **32**, 170-173 (2011).
2. D. Y. Zhang, A. J. Turberfield, B. Yurke, E. Winfree, Engineering Entropy-Driven Reactions and Networks Catalyzed by DNA. *Science* **318**, 1121-1125 (2007).
3. R. J. Macfarlane *et al.*, Nanoparticle Superlattice Engineering with DNA. *Science* **334**, 204-208 (2011).
4. R. Jin, G. Wu, Z. Li, C. A. Mirkin, G. C. Schatz, What Controls the Melting Properties of DNA-Linked Gold Nanoparticle Assemblies? *J. Am. Chem. Soc.* **125**, 1643-1654 (2003).
5. J. D. Brodin, E. Auyeung, C. A. Mirkin, DNA-mediated engineering of multicomponent enzyme crystals. *Proc. Natl. Acad. Sci. U. S. A.* **112**, 4564-4569 (2015).
6. K. Krishnamoorthy *et al.*, Defining the Structure of a Protein–Spherical Nucleic Acid Conjugate and Its Counterionic Cloud. *ACS Cent. Sci.* **4**, 378-386 (2018).
7. T. Samejima, J. T. Yang, Reconstitution of Acid-denatured Catalase. *J. Biol. Chem.* **238**, 3256-3261 (1963).
8. R. J. Macfarlane *et al.*, Importance of the DNA "bond" in programmable nanoparticle crystallization. *Proc. Natl. Acad. Sci. U.S.A.* **111**, 14995-15000 (2014).
9. W. B. Rogers, V. N. Manoharan, Programming colloidal phase transitions with DNA strand displacement. *Science* **347**, 639-642 (2015).
10. W. B. Rogers, J. C. Crocker, Direct measurements of DNA-mediated colloidal interactions and their quantitative modeling. *Proc. Natl. Acad. Sci. U.S.A.* **108**, 15687-15692 (2011).
11. P. L. Biancaniello, A. J. Kim, J. C. Crocker, Colloidal Interactions and Self-Assembly Using DNA Hybridization. *Phys. Rev. Lett.* **94**, 058302 (2005).
12. S. E. Seo, T. Li, A. J. Senesi, C. A. Mirkin, B. Lee, The Role of Repulsion in Colloidal Crystal Engineering with DNA. *J. Am. Chem. Soc.* **139**, 16528-16535 (2017).